

## A Neural Theory of Circadian Rhythms: The Gated Pacemaker

Gail A. Carpenter\*<sup>1</sup> and Stephen Grossberg\*\*<sup>2</sup>

<sup>1</sup> Department of Mathematics, Northeastern University, and Center for Adaptive Systems, Department of Mathematics, Boston University, Boston, MA, USA

<sup>2</sup> Center for Adaptive Systems, Department of Mathematics, Boston University, Boston, MA, USA

**Abstract.** This article describes a behaviorally, physiologically, and anatomically predictive model of how circadian rhythms are generated by each suprachiasmatic nucleus (SCN) of the mammalian hypothalamus. This gated pacemaker model is defined in terms of competing on-cell off-cell populations whose positive feedback signals are gated by slowly accumulating chemical transmitter substances. These components have also been used to model other hypothalamic circuits, notably the eating circuit. A parametric analysis of the types of oscillations supported by the model is presented. The complementary reactions to light of diurnal and nocturnal mammals as well as their similar phase response curves are obtained. The “dead zone” of the phase response curve during the subjective day of a nocturnal rodent is also explained. Oscillations are suppressed by high intensities of steady light. Operations that alter the parameters of the model transmitters can phase shift or otherwise change its circadian oscillation. Effects of ablation and hormones on model oscillations are summarized. Observed oscillations include regular periodic solutions, periodic plateau solutions, rippled plateau solutions, period doubling solutions, slow modulation of oscillations over a period of months, and repeating sequences of oscillation clusters. The model period increases inversely with the transmitter accumulation rate but is insensitive to other parameter choices except near the breakdown of oscillations. The model’s clocklike nature is thus a mathematical property rather than a

formal postulate. A singular perturbation approach to the model’s analysis is described.

### 1 Introduction

#### *A A Physiological Model of a Circadian Pacemaker*

Circadian rhythms occur in a wide variety of mammalian physiological systems. Moore-Ede et al. (1982) have, for example, written that “as the documentation of rhythms in various human physiological systems proceeded apace, it became apparent that it was often more significant to find no circadian rhythm in a physiological variable than to find one” (p. 16). Despite the widespread occurrence of circadian properties, the physiological mechanisms that generate circadian rhythms have yet to be characterized. In every mammal studied so far, a pacemaker for the control of the wake-sleep and activity-rest cycles has been located in the pair of suprachiasmatic nuclei (SCN) of the hypothalamus (Moore, 1973, 1974). This article defines and analyses a behaviorally, physiologically, and anatomically predictive model of the SCN circadian pacemaker. We call this model the *gated pacemaker* model due to the central role played by transmitter gating actions in generating the model’s circadian rhythm (Carpenter and Grossberg, 1983a).

Some of the gated pacemaker’s behavioral properties are the following. Although both nocturnal mammals and diurnal mammals possess a pacemaker within their SCN, these animals react to the daily light-dark cycle in a complementary fashion (Moore-Ede et al., 1982). We show that the same model mechanisms can be used to produce these complementary reactions, as well as the similar phase response curves of nocturnal and diurnal mammals in response to pulses of light. The diurnal gated pacemaker can generate approximately 48-h days (period doubling) when it is placed into dim steady light, as occasionally happens

\* Supported in part by the Air Force Office of Scientific Research (AFOSR 82-0148), the National Science Foundation (NSF MCS-82-07778), the Northeastern University Research and Scholarship Development Fund, and the Office of Naval Research (ONR-N00014-83-K0337)

\*\* Supported in part by the Air Force Office of Scientific Research (AFOSR 82-0148), the National Science Foundation (NSF IST-80-00257), and the Office of Naval Research (ONR-N00014-83-K0337)

to humans who live in caves for long periods of time (Jouvet et al., 1974). The circadian rhythm of the diurnal model can be suppressed by intense steady light. Aschoff (1979, p. 238) writes about this property that "at high intensities of illumination circadian systems often seem to break down, as primarily exemplified by arrhythmicity in records of locomotor activity." Biorhythms on a time scale of months have been observed superimposed on the model's circadian rhythm. Very complex breakdown of the model's circadian rhythmicity, suggestive of chaos, have also been observed. Some of these oscillatory waveforms are of independent mathematical interest due to their novel properties.

Since each of the model's mechanisms has a physiological interpretation, the parameter ranges in which the above behaviors occur suggest tests of the model by predicting how prescribed physiological manipulations may alter circadian properties of behavior. The model's physiological interpretation suggests a set of predictions that are of particular importance. Chemical transmitters form a part of the gated pacemaker. Many neural transmitters are known to oscillate with a circadian rhythm (Naber et al., 1981; Kafka et al., 1981). The model's transmitters oscillate because their gating action forms part of the pacemaker mechanism, not merely because they are driven by a separate pacemaker. If chemical transmitters play a role in the SCN pacemaker, then a potent antagonist of these transmitters should abolish the SCN rhythm. The role of chemical transmitters in the gated pacemaker is also compatible with the fact that antidepressant drugs can alter the mood of manic-depressive patients by modifying their wake-sleep circadian cycle (Wehr et al., 1979; Kafka et al., 1982; Wehr and Wirz-Justice, 1982).

The model's anatomical interpretation suggests another set of predictions. These predictions describe effects on gated pacemaker activity of cutting out one of the two SCN or part of each SCN, or of severing the neural pathways that join the two SCN through the optic chiasm (Carpenter and Grossberg, 1983b; Sisk and Turek, 1982).

### *B Multiple Oscillators from Similar Mechanisms*

The model oscillators are built up from mechanisms that have been used to analyse other phenomena, such as eating and drinking (Grossberg, 1982a, 1983a), that are known to be mediated by the hypothalamus (Olds, 1977). We therefore suggest that the hypothalamic circuits that control different types of emotion-related behaviors may all be built up from similar physiological components. This hypothesis may prove helpful in characterizing the hypothalamic circuit that controls the human temperature rhythm (Wever, 1979) as well

as hypothalamically mediated rhythmic properties of the eating cycle (Rosenwasser et al., 1981; Moore-Ede et al., 1982).

### *C Metabolic Feedback and Slow Gain Control*

In this article, we focus on the model's circadian pacemaker. The full circadian model augments the gated pacemaker with two auxiliary processes. Each of these auxiliary processes is driven by the pacemaker and modulates the pacemaker activity via feedback signalling (Carpenter and Grossberg, 1983a, b).

One of these processes regulates a metabolic feedback signal: the gated pacemaker generates behavioral activity which, in turn, produces a feedback signal to the pacemaker that serves as a metabolic index of fatigue. We use this metabolic feedback signal to explain how the circadian activity rhythm can split into two components either due to appropriate lighting conditions (Pittendrigh, 1960; Hoffman, 1971; Earnest and Turek, 1982; Pickard and Turek, 1982) or to hormones in the bloodstream (Gwinner, 1974). In the homologous model circuit that is used to analyse eating behavior, the metabolic feedback signal is replaced by a satiety signal that also acts through the bloodstream (Grossberg, 1982a, 1983a). Aschoff's rule (Aschoff, 1979) is observed in the model due to two factors operating together. The activation of nocturnal model off-cells by light plus the action of metabolic feedback on the off-cells leads to examples (Carpenter and Grossberg, 1983b) wherein the duration of behavioral activity decreases and the total period increases as the steady light level is parametrically increased. The activation of diurnal model on-cells by light plus the action of metabolic feedback on the off-cells leads to examples wherein the duration of behavioral activity increases and the total period decreases as the steady light level is parametrically increased. Exceptions to Aschoff's rule are more common in the diurnal model than in the nocturnal model, as also occurs *in vivo*, due to the asymmetric role of metabolic feedback relative to the site of action of the light input within the diurnal and nocturnal models (Carpenter and Grossberg, 1983b).

The second auxiliary process is a slowly varying gain control process that buffers the model's reaction to adventitious lighting changes, such as cloudy weather, and alters the model's properties in response to statistically reliable lighting changes, such as seasonal fluctuations. We use this slow gain control process to explain the slow onset of split rhythms and the several types of long-term after-effects that prior lighting conditions can have on subsequent activity cycles (Pittendrigh, 1974). In the homologous model circuit that is used to analyse eating behavior, the slow gain

control process is replaced by conditionable signals that are activated by food-related cues.

The correspondences between the model SCN circuit and eating circuit support the hypothesis that similar mechanisms are adapted to specialized functions within the hypothalamus.

#### D Comparison with other Pacemaker Models

Previous models of circadian rhythms have been defined in terms of oscillators that were originally developed to explain non-circadian phenomena. A pair of coupled van der Pol oscillators has been used to model interactions between the activity-rest pacemaker and the temperature pacemaker of humans (Kronauer et al., 1982). Our results complement this study by suggesting a physiological model for each pacemaker.

A pair of coupled FitzHugh-Nagumo oscillators (FitzHugh, 1960; Nagumo et al., 1961) has been used to analyse the splitting of the circadian rhythm (Kawato and Suzuki, 1980). This model faces several difficulties. The FitzHugh-Nagumo model is a simplified version of the Hodgkin-Huxley model of nerve impulse propagation. As such, its physical time scale is in the millisecond range rather than the circadian range. As Kawato and Suzuki have noted, "the BVP (van der Pol) equation and Nagumo's equation were derived for neural rhythms with much shorter periods than 24 h. However, in the absence of information regarding the state variables relevant to circadian pacemakers, we use the abstract model" (p. 557).

A second difficulty of the FitzHugh-Nagumo coupled oscillator model concerns its explanation of split rhythms. Split rhythms are caused in the Kawato-Suzuki model when its two oscillators become out-of-phase with each other. This happens because light is assumed to strengthen the inhibitory coupling between the oscillators. In order to explain splitting in both nocturnal and diurnal animals using this approach, one would need to suppose that light strengthens the inhibitory coupling between the oscillators of a nocturnal model and weakens the inhibitory coupling between the oscillators of a diurnal model. Moreover, the inhibitory coupling between oscillators would have to be weak when the nocturnal model is in the dark and when the diurnal model is in the light, so that splitting does not routinely occur under these conditions. These formal hypotheses do not seem to play any role in the model except to cause split rhythms.

The gated pacemaker model avoids these interpretive difficulties as follows. The time scale difficulties are avoided due to the role of slowly accumulating transmitter substances in generating the gated pacemaker rhythm. Our split rhythm explanation does not

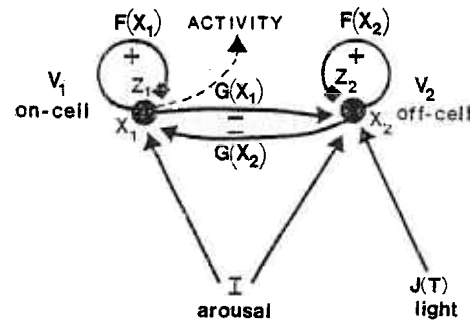


Fig. 1. Anatomy and physiology of a gated pacemaker. The potential  $X_1$  of an on-cell (population) and the potential  $X_2$  of an off-cell (population) obey membrane Eqs. (1) and (2), respectively. Transmitter substance  $Z_1$  gates the positive feedback signal  $F(X_1)$  from the on-cell (population) to itself, and transmitter substance  $Z_2$  gates the positive feedback signal  $F(X_2)$  from the off-cell (population) to itself. Term  $I$  is the nonspecific arousal level, which is held constant during the simulations reported herein. The off-cells inhibit the on-cells via signal  $G(X_2)$  in (1), and the on-cells inhibit the off-cells via signal  $G(X_1)$  in (2). The light input  $J(T)$  excites the off-cells (nocturnal model). The transmitter  $Z_1$  in (3) accumulates via term  $D(E - Z_1)$  and is released at rate  $-KF(X_1)Z_1$  by gating the signal  $F(X_1)$ . A similar law governs  $Z_2$  in (4). Many basic model properties persist in modified versions of equations (1)–(4). Species-specific variations and future data may support particular versions without altering the qualitative explanations of model properties

hypothesize a light-sensitive coupling strength between SCN oscillators. Instead, we show how the metabolic feedback process, which plays a physically important role, can cause splits under certain circumstances.

## 2. The Gated Pacemaker

The gated pacemaker model describes the dynamics of on-cell/off-cell pairs, called *gated dipoles*, in which the on-cells and the off-cells mutually inhibit one another. Populations of these gated dipoles are assumed to exist in each SCN. The following processes define a gated pacemaker (Fig. 1):

- 1) slowly accumulating transmitter substances are depleted by gating the release of feedback signals;
- 2) the feedback signals are organized as an on-center off-surround, or competitive, anatomy;
- 3) both on-cells and off-cells are tonically aroused;
- 4) light excites the on-cells of a diurnal model and the off-cells of a nocturnal model;
- 5) the on-cells drive observable activity, such as wheel-turning, in both the diurnal model and the nocturnal model.

The model equations for a nocturnal gated pacemaker are

$$\frac{dX_1}{dT} = -AX_1 + (B - X_1)[I + F(X_1)Z_1] - (X_1 + C)G(X_2), \quad (1)$$

$$\frac{dX_2}{dT} = -AX_2 + (B - X_2)[I + F(X_2)Z_2 + J(T)] - (X_2 + C)G(X_1). \quad (2)$$

$$\frac{dZ_1}{dT} = D(E - Z_1) - KF(X_1)Z_1, \quad (3)$$

$$\frac{dZ_2}{dT} = D(E - Z_2) - KF(X_2)Z_2. \quad (4)$$

Variable  $X_1$  in Eq. (1) is the potential of an on-cell (population)  $V_1$ . Variable  $X_2$  in Eq. (2) is the potential of an off-cell (population)  $V_2$ . Both  $X_1$  and  $X_2$  obey membrane equations (Hodgkin, 1964; Katz, 1966; Kuffler and Nicholls, 1976; Plonsey, 1969). In (1) and (2), the parameter  $-A$  in the terms  $-AX_1$  and  $-AX_2$  determines the fast decay rate of the potentials  $X_1$  and  $X_2$ . Also in (1) and (2), term  $I$  represents the arousal level that equally excites  $V_1$  and  $V_2$ . In (1), the transmitter substance  $Z_1$  gates the nonnegative feedback signal  $F(X_1)$  from  $V_1$  to itself. Term  $F(X_1)Z_1$  is proportional to the rate at which transmitter is released from the feedback pathway from  $V_1$  to itself, thereby re-exciting  $X_1$ . The off-cells  $V_2$  inhibit the on-cells  $V_1$  via the nonnegative signal  $G(X_2)$  in term  $-(X_1 + C)G(X_2)$  of (1). Equation (2) is the same as Eq. (1), except that the indices 1 and 2 are interchanged, and the light input  $J(T)$  excites  $V_2$ , but not  $V_1$ , because system (1)–(4) represents a nocturnal model.

Equations (3) and (4) define the transmitter processes  $Z_1$  and  $Z_2$ . In (3), the transmitter  $Z_1$  accumulates to its maximal level  $E$  at a slow rate  $D$  via the term  $D(E - Z_1)$ . This slow accumulation process is balanced by the release of  $Z_1$  at rate  $KF(X_1)Z_1$ , leading to the excitation of  $X_1$  in Eq. (1). A similar combination of slow accumulation and gated release defines the dynamics of transmitter  $Z_2$  in (4).

In all, system (1)–(4) describes a four-dimensional fast-slow process in which two fast potentials interact with two slow auxiliary processes. By comparison, the Hodgkin-Huxley model of nerve impulse transmission (Hodgkin and Huxley, 1952) is also a four-dimensional fast-slow process, but one in which just one potential interacts with three auxiliary processes (Carpenter and Grossberg, 1983a). Also the accumulation rate of the two slow transmitter processes in the gated pacemaker model is assumed to be substantially slower than the reaction rates of the ionic processes that couple to the Hodgkin-Huxley potential.

The dimensionless model equations corresponding to Eqs. (1)–(4) are:

$$\frac{dx_1}{dt} = -x_1 + (1 - x_1)[C_1 + C_2 f(x_1)z_1] - (x_1 + C_3)C_4 g(x_2), \quad (5)$$

$$\frac{dx_2}{dt} = -x_2 + (1 - x_2)[C_1 + C_2 f(x_2)z_2 + L(t)] - (x_1 + C_3)C_4 g(x_1), \quad (6)$$

$$\frac{dz_1}{dt} = C_5[1 - z_1 - C_6 f(x_1)z_1], \quad (7)$$

and

$$\frac{dz_2}{dt} = C_5[1 - z_2 - C_6 f(x_2)z_2]. \quad (8)$$

The symbols in the dimensionless system (5)–(8) are related to the symbols in the defining system (1)–(4) by the following identities:

*Variables*

$$x_1 = \frac{X_1}{B}, \quad (9)$$

$$x_2 = \frac{X_2}{B},$$

$$z_1 = \frac{Z_1}{E},$$

$$z_2 = \frac{Z_2}{E},$$

$$t = AT. \quad (13)$$

*Constants*

$$C_1 = \frac{I}{A},$$

$$C_2 = \frac{EF_{\max}}{A},$$

where

$$F_{\max} = \max(F),$$

$$C_3 = \frac{C}{B},$$

$$C_4 = \frac{G_{\max}}{A},$$

where

$$G_{\max} = \max(G),$$

$$C_5 = \frac{D}{A},$$

$$C_6 = \frac{KF_{\max}}{D}$$

## Functions

$$f(w) = \frac{F(Bw)}{F_{\max}} \quad (22)$$

$$g(w) = \frac{G(Bw)}{G_{\max}} \quad (23)$$

and

$$L(t) = \frac{J(t/A)}{A} \quad (24)$$

Note that the feedback signals  $f(w)$  and  $g(w)$  in (22) and (23) are scaled so that  $0 \leq f \leq 1$  and  $0 \leq g \leq 1$ . These signals are chosen to be either a sigmoid ( $S$ -shaped) function of activity, such as

$$f(w) = \begin{cases} \frac{w^2}{C_7^2 + w^2} & \text{if } w \geq 0 \\ 0 & \text{if } w < 0, \end{cases} \quad (25)$$

or a threshold-linear function (linear above a threshold cut-off), such as

$$g(w) = \begin{cases} w & \text{if } 0 \leq w \leq 1 \\ 0 & \text{if } w < 0 \end{cases} \quad (26)$$

### 3 Qualitative Basis of Oscillations

An intuitive understanding of why a gated pacemaker oscillates, and of how to choose system parameters, may be derived from the following qualitative remarks. Suppose that the system starts out with  $x_1$  large and  $x_2$  small, but with both transmitters fully accumulated, so that  $z_1 \cong 1$  and  $z_2 \cong 1$ . At first,  $x_1$  maintains its advantage over  $x_2$ , as follows. Because  $x_1$  is large and  $z_1 \cong 1$ , the feedback signal  $f(x_1)z_1$  from  $V_1$  to itself is large, as is the negative feedback signal  $g(x_1)$  from  $V_1$  to  $V_2$ . Because  $f(x_1)$  is large, however,  $z_1$  is slowly depleted at the rate  $-C_5 C_6 f(x_1)z_1$ , by (7). Consequently, the gated signal  $f(x_1)z_1$  gradually becomes small despite the fact that  $x_1$  remains large.

As this is going on,  $x_2$  and its feedback signal  $f(x_2)$  remain small, so that the transmitter release rate  $-C_5 C_6 f(x_2)z_2$  in (8) also remains small. Consequently,  $z_2$  remains large as  $z_1$  is gradually depleted. As a result of these changes, the positive feedback term

$$(1-x_1)[C_1 + C_2 f(x_1)z_1] \quad (27)$$

in (5) diminishes relative to the positive feedback term

$$(1-x_2)[C_1 + C_2 f(x_2)z_2] \quad (28)$$

in (6), even though  $x_1$  remains larger than  $x_2$ .

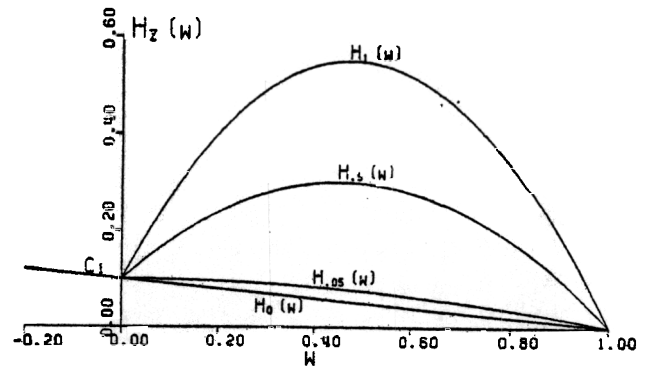


Fig. 2. The family of positive feedback functions  $H_z(w)$ . At intermediate values of  $x_1$ ,  $H_{z_1}(x_1) > C_1$  if  $z_1$  is sufficiently close to 1, whereas  $C_1 > H_{z_1}(x_1)$  if  $z_1$  is sufficiently close to 0. At small values of  $x_2$ ,  $H_{z_2}(x_2) \cong C_1$  for all  $z_2$ ,  $0 \leq z_2 \leq 1$ . Consequently, as  $z_1$  decreases from large to small values, the function  $H_{z_1}(x_1) - H_{z_2}(x_2)$  decreases until a switch in the relative sizes of  $x_1$  and  $x_2$  is initiated

This relative change can be understood more precisely by graphing the function

$$H_z(w) = (1-w)[C_1 + C_2 f(w)z] \quad (29)$$

at extreme values  $z=0$  and  $z=1$  of the parameter  $z$  (Fig. 2). The function  $H_0(w)$  decreases linearly from  $C_1$  to 0 as  $w$  increases from 0 to 1, no matter how  $f(w)$  is chosen. The function  $f(w)$  is chosen so that the graph of  $H_1(w)$  increases from  $H_1(0) = C_1$  to a maximum before decreasing to  $H_1(1) = 0$ . For example, if

$$f(w) = \begin{cases} w & \text{if } w \geq 0 \\ 0 & \text{if } w < 0, \end{cases} \quad (30)$$

then these properties of  $H_1(w)$  hold if and only if

$$C_1 < C_2. \quad (31)$$

By Fig. 2, if  $x_2$  is sufficiently small, then  $H_{z_2}(x_2) \cong C_1$  no matter how  $z \in [0, 1]$  is chosen. In particular, if  $z = z_2 \cong 1$ , then  $H_{z_2}(x_2) \cong C_1$ . By contrast, if  $x_1$  is fairly large, then the inequalities

$$H_1(x_1) > C_1 \quad (32)$$

and

$$H_0(x_1) < C_1 \quad (33)$$

hold. In other words, if  $x_1$  and  $x_2$  remain approximately constant while  $x_1 > x_2$  and  $x_2 \cong 0$ , then the relative sizes of (27) and (28) can reverse as  $z_1$  is depleted.

Due to the relatively large decrease in the positive feedback term (27) in (5),  $x_1$  itself begins to decrease, as does  $g(x_1)$  in (6). The positive feedback term

$$(1-x_2)[C_1 + C_2 f(x_2)z_2] \quad (28)$$

from  $V_2$  to itself in (6) can therefore begin to overcome the negative feedback term

$$-(x_2 + C_3)C_4 g(x_1) \quad (34)$$

**Table 1.** Typical parameter values for a threshold-linear nocturnal pacemaker

$C_1 =$	0.10
$C_2 =$	2.00
$C_3 =$	0.10
$C_4 =$	5.00
$C_5 =$	0.01
$C_6 =$	10.00

in (6), and  $x_2$  begins to grow. At first, the growth of  $x_2$  does not depend upon the size of  $z_2$ , because if  $x_2$  is small then  $H_z(x_2) \cong C_1$  no matter how  $z$  is chosen. As  $x_2$  begins to increase, however, the *continued* increase of  $x_2$  depends crucially upon the fact that  $z_2$  is large, due to the different graphs of  $H_1(w)$  and  $H_0(w)$  at middle values of  $w$ . Since  $z_2$  is large when  $x_2$  begins to grow, a switch in the relative sizes of  $x_1$  and  $x_2$  occurs. As  $x_2$  becomes large, it suppresses  $x_1$  via the large negative feedback signal  $g(x_2)$ . Now  $x_2$  has the advantage, and the competitive cycle starts to repeat itself as  $z_2$  is progressively depleted and  $z_1$  is replenished.

#### 4 Parameter Estimation

The parameters  $C_1, C_2, \dots, C_6$  are chosen to guarantee that the qualitative properties described in Section 3 occur. The parameters need to be chosen so that no one term in system (5)–(8) dominates any of the others. It turns out that a broad range of parameters can accomplish this goal. We first show that some simple balancing rules lead to a successful choice of parameters. Then we illustrate the robustness of this parameter choice by varying each parameter separately while the others are held fixed.

The parameters in Table 1 are arrived at as follows. Consider the positive feedback term

$$(1 - x_1)[C_1 + C_2 f(x_1)z_1] \quad (27)$$

of (5). We want to balance the terms  $C_1$  and  $C_2 f(x_1)z_1$  to prevent either term from totally dominating the other in all system states. To fix ideas, let  $f(x_1) = \max(x_1, 0)$ . Since by (5),  $-C_3 \leq x_1 \leq 1$ , it follows that  $0 \leq f(x_1) \leq 1$ . Also by (7),  $0 \leq z_1 \leq 1$ . In all,  $C_2$  is multiplied by a variable term that is always less than 1. As a first approximation, we therefore need to choose  $C_1 < C_2$ , as in (31).

A more precise restriction upon  $C_1$  and  $C_2$  is needed, because we want  $C_2 f(x_1)z_1$  to exceed  $C_1$  some of the time but not all of the time. To achieve this property, suppose on the average that  $x_1 \cong 0.2$ ,  $x_2 \cong 0.2$ ,  $z_1 \cong 0.7$ , and  $z_2 \cong 0.7$ . These scalesetting estimates are suggested by the facts that  $x_1$  and  $x_2$  in (5) and (6), respectively, are each affected by two negative

terms that tend to drive them towards zero, whereas  $z_1$  and  $z_2$  in (7) and (8), respectively, tend to accumulate towards 1 when they are not being depleted by a gating action. These average estimates imply that

$$C_2 f(x_1)z_1 \cong (0.14)C_2 \quad (35)$$

on the average. In order to keep term  $C_2 f(x_1)z_1$  bigger than  $C_1$  some of the time, we choose

$$C_2 = 20C_1, \quad (36)$$

since then

$$C_2 f(x_1)z_1 \cong 2.8C_1 \quad (37)$$

on the average.

In order to choose  $C_1$ , we consider term

$$-x_1 + (1 - x_1)[C_1 + C_2 f(x_1)z_1] \quad (38)$$

of (5). We want the positive feedback term (27) to exceed the decay term  $-x_1$  some of the time. If we choose

$$C_1 = 0.1, \quad (39)$$

and thus by (36)

$$C_2 = 2, \quad (40)$$

then using the average estimates  $x_1 \cong 0.2$  and  $z_1 \cong 0.7$ , (38) is approximately equal to

$$-0.2 + 0.3 > 0, \quad (41)$$

which achieves a satisfactory balance of terms. [In (39),  $C_1$  could be chosen significantly larger, provided subsequent terms are balanced properly. For example, oscillations can also occur when  $C_1 = 0.5$  and  $C_2 = 10$ .]

The parameters  $C_3$  and  $C_4$  in the negative feedback term

$$-(x_1 + C_3)C_4 g(x_2) \quad (42)$$

are chosen as follows. By (17), parameter  $C_3 = C/B$ . In a membrane equation such as (1) or (2), parameter  $B$  equals the sodium saturation point and  $C$  equals the potassium saturation point. In vivo,  $B$  is often ten times larger than  $C$  (Hodgkin and Huxley, 1952). Hence we choose

$$C_3 = 0.1. \quad (43)$$

We choose  $C_4$  so that the positive feedback term (27) and the negative feedback term (42) can alternately be smaller or larger than one another. Letting  $g(x_2) = \max(x_2, 0)$  for definiteness, (42) is approximately  $(0.06)C_4$ . If we let

$$C_4 = 5 \quad (44)$$

then (42) approximately equals 0.3, which balances the estimate of (27) that appears in (41).

To choose  $C_5$ , we observe by (20) that  $C_5$  is the ratio of  $D$  to  $A$ . Since the transmitter accumulation rate ( $D$ ) is much slower than the decay rate ( $A$ ) of the potentials,  $C_5 \ll 1$ . For definiteness, we choose

$$C_5 = 0.01. \quad (45)$$

Parameter  $C_6$  is chosen as follows. First, we want the rate  $-C_5 C_6$  of transmitter depletion in (7) and (8) to be slower than the unit decay rate of the potential; that is

$$C_5 C_6 = (0.01)C_6 < 1. \quad (46)$$

Second, we want the gated signal  $C_2 f(x_1)z_1$  in (5) to decrease significantly as  $z_1$  is maximally depleted and  $x_1$  remains large. By (7), if  $z_1$  equilibrates to  $f(x_1)$ , then

$$z_1 \cong \frac{1}{1 + C_6 f(x_1)}. \quad (47)$$

If  $x_1$  is estimated by its maximum value of 1, then

$$z_1 \cong \frac{1}{1 + C_6}. \quad (48)$$

If we choose

$$C_6 = 10, \quad (49)$$

then (46) is valid because  $0.1 < 1$ . Also a significant decrease in  $C_2 f(x_1)z_1$  can be achieved since, by (48), the minimal value of  $z_1$  is approximately 0.09.

### 5 A Typical Oscillation in the Dark

This section describes the oscillations that occur with parameters chosen as in Table 1 and no light inputs (free-run in the dark). Due to the fact that system (5)–(8) is four-dimensional, we plot its solutions in three different ways. In Fig. 3a, each of the variables  $x_1$  and  $z_1$  is plotted through time. In Fig. 3b, both pairs  $(x_1, z_1)$  and  $(x_2, z_2)$  are plotted in the  $(x, z)$  coordinate plane through time. In Fig. 3c, each of the variables  $x_1$  and  $x_2$  is plotted through time.

Figure 3a illustrates how  $z_1$  accumulates while  $x_1$  is small. This figure also shows that the graph of  $x_1$  exhibits an overshoot shortly after  $x_1$  reaches its maximum. This overshoot is due to the multiplicative form of the feedback signal  $f(x_1)z_1$  (Carpenter and Grossberg, 1981; Grossberg, 1968, 1981, 1983a). Term  $f(x_1)z_1$  reaches its maximum value when  $x_1$  and  $z_1$  are large. Then  $z_1$  starts to deplete so the product  $f(x_1)z_1$  also decreases. As a result,  $x_1$  decreases to a plateau value until the balance of terms that was described in Sect. 3 causes a rapid switch to occur in the relative sizes of  $x_1$  and  $x_2$ .

Figure 3b shows that the two pairs  $(x_1, z_1)$  and  $(x_2, z_2)$  approach the same limit cycle from their dis-

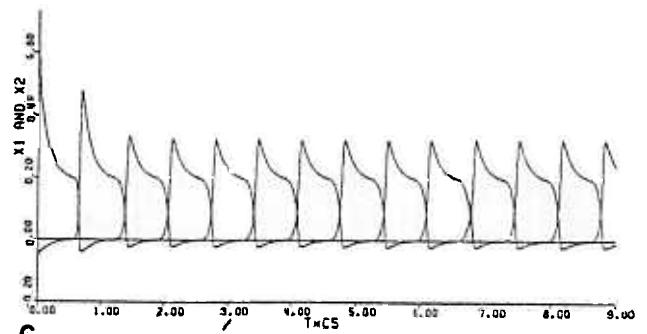
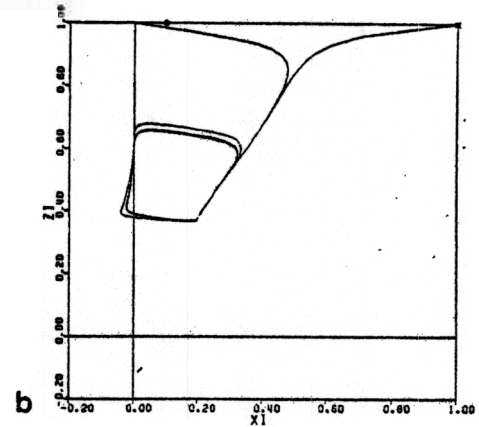
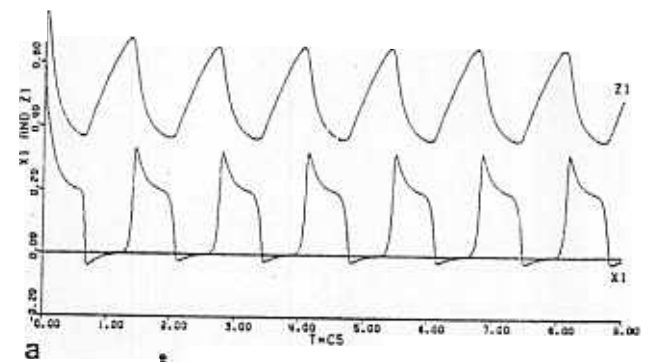


Fig. 3a–c. Three ways to plot gated pacemaker trajectories. a Functions  $x_1(t)$  and  $z_1(t)$  are plotted through time. b The phase portraits of  $(x_1(t), z_1(t))$  and  $(x_2(t), z_2(t))$  are plotted through time in  $(x, z)$  coordinates. c Functions  $x_1(t)$  and  $x_2(t)$  are plotted through time. Parameters are chosen as in Table 1

tinct initial values in  $(x, z)$  space. Figure 3c shows that the  $x_1$  and  $x_2$  potentials are out-of-phase with each other near this limit cycle. In particular, the rapid decay of  $x_1$  occurs during the rapid rise of  $x_2$ , and conversely.

### 6 Phase Response Curves in Diurnal and Nocturnal Gated Pacemakers

In the gated pacemaker model, the assumption that light inputs excite the on-cells of diurnal animals and the off-cells of nocturnal animals is compatible with the familiar day activity of diurnal animals and night

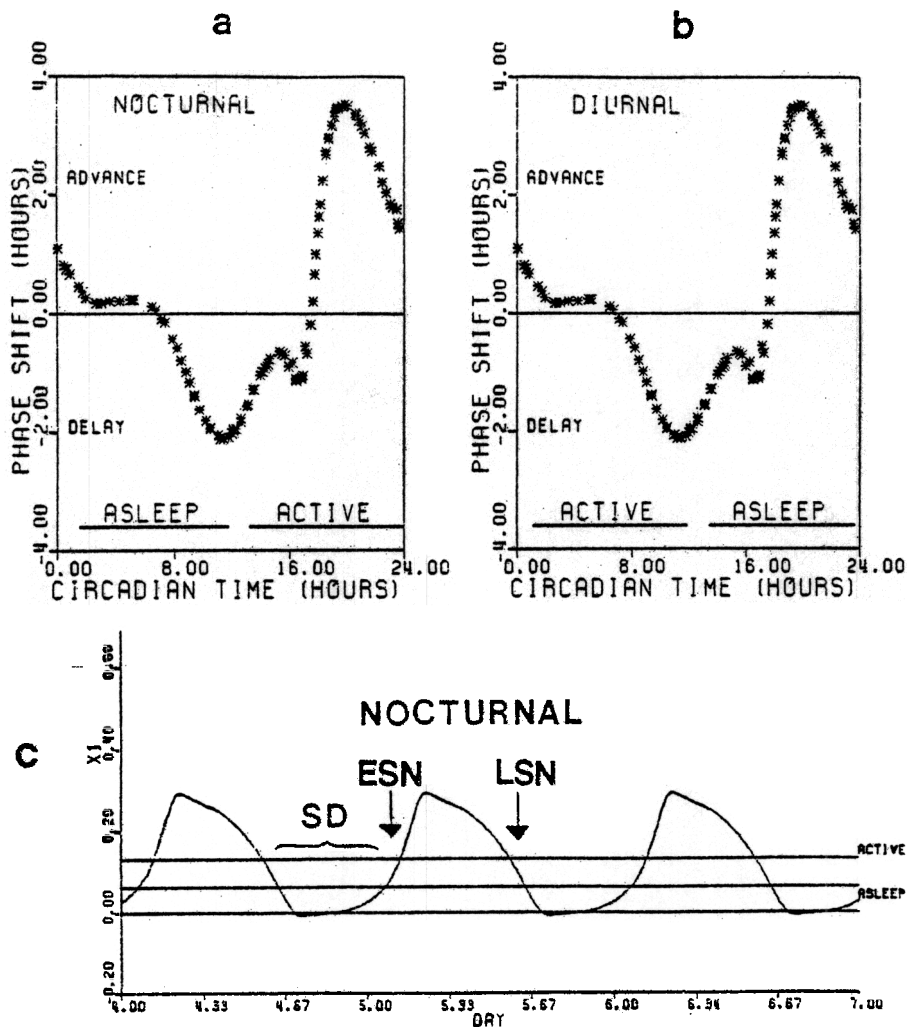


Fig. 4a-c. Phase response curves of nocturnal and diurnal gated pacemakers. **a** A typical phase response curve for a nocturnal pacemaker. Parameters are chosen as in Table 1, except that  $C_1 = 0.13$ . Light pulses of dimensionless intensity 0.1 were flashed for 30 min. **b** A typical phase response curve for a diurnal pacemaker. Parameters are chosen as in **a**. **c** The on-cell potential  $x_1(t)$  of a nocturnal pacemaker is plotted as a function of time. Small values correspond to sleep ( $x_1(t) \leq C_8$ ) and large values correspond to the waking state. The model is asleep during the day and awake at night. The "subjective day" (SD), "early subjective night" (ESN), and "late subjective night" (LSN) of the model are defined accordingly.

activity of nocturnal animals. Although these hypotheses generate complementary activity cycles in response to a daily cycle of light-dark episodes, they also imply that isolated light pulses delivered to an animal living in the dark reset the phases of both diurnal and nocturnal models in a similar way, as the data demand (DeCoursey, 1960; Pittendrigh, 1960; Kramm, 1971; Daan and Pittendrigh, 1976; Pohl, 1982). This property of gated pacemakers contrasts with the explanation of phase resetting that is suggested when van der Pol oscillators are used to model the pacemaker. The latter approach suggests that complementary reactions to light of diurnal and nocturnal animals are controlled by interactions that occur beyond the SCN pacemaker stage. As Moore-Ede, Sulzman, and Fuller (1982, pp.81-82) have noted:

"The circadian systems of diurnal and nocturnal species must be organized differently to account for the dramatic differences in the phase relationships of their rhythms to the light-dark cycle (i.e., day-active vs. night-active). It is possible that the differences lie in the coupling between zeitgeber and pacemaker. However, ... the similarities between nocturnal and diurnal species in the way that light resets circadian pacemakers (i.e., the phase response curves) makes it more likely that the difference in the phase relationships of the rhythms of nocturnal and diurnal animals actually depends on differences in the coupling mechanisms between the circadian pacemaker and the rhythms it drives."

Figure 4 depicts the phase response curves of diurnal and nocturnal gated pacemakers in response to

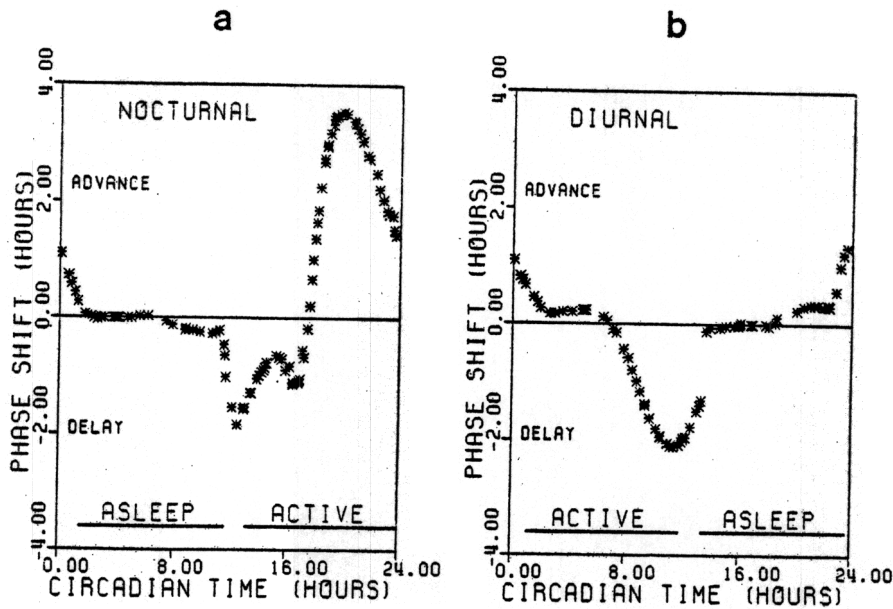


Fig. 5a and b. Phase response curves of nocturnal and diurnal gated pacemakers with light attenuation during sleep. a A typical phase response curve for a nocturnal pacemaker with  $\theta=0.1$ . All other parameters are chosen as in Fig. 4. b A typical phase response curve for a diurnal pacemaker with all parameters chosen as in a

light pulses. These curves indicate that complementary light-dark cycles and similar phase response curves can coexist at the SCN level if these structures are built up from gated pacemakers. The similar phase response curves of diurnal and nocturnal models are intuitively explained as follows.

During the "early subjective night" of a model diurnal animal, a light pulse that excites the on-cell prolongs its active phase, delays the rest cycle, and thereby causes a phase delay. During the "early subjective night" of a model nocturnal animal, a light pulse that excites the off-cell prolongs its active phase, delays the ensuing activity cycle, and again creates a phase delay. During the "late subjective night" of a diurnal animal, a light pulse that excites the on-cell induces a premature onset of on-cell activity, thereby causing a phase advance in the onset of activity. During the "late subjective night" of a nocturnal model animal, a light pulse that excites the off-cell induces a premature onset of off-cell activity, thereby causing a phase advance in the onset of the next activity cycle. A light pulse during the "subjective day" of either a diurnal or a nocturnal model has relatively little effect.

One way to test whether a gated pacemaker controls phase resetting in vivo is to parametrically excite or inhibit the pacemaker transmitter while the phase resetting light pulse is active. A combination of drugs and light pulses may accomplish this joint manipulation. Then predictable changes in the phase response curves beyond those obtainable with a light pulse alone should occur. Such an experimental result could not be explained by a formal oscillator model.

Some details about how the phase response curves are generated are worthy of note. During a diurnal

animal's subjective night, for example, both phase advances and phase delays can be caused by light pulses (Kramm, 1971; Pohl, 1982). Thus light pulses that occur while the animal is asleep can alter its circadian rhythm, so that light can affect the animal's pacemaker even when its eyes are closed.

The gated pacemaker model incorporates this property in terms of the following hypothesis. If  $L^*(t)$  is the light signal that reaches the SCN when the eyes are open, we define the light input  $L(t)$  in Eq. (6) at all times by

$$L(t) = \begin{cases} L^*(t) & \text{if model is awake} \\ \theta L^*(t) & \text{if model is asleep,} \end{cases} \quad (50)$$

where  $0 < \theta \leq 1$ . In Fig. 4,  $\theta = 1$ . The form of the phase response curves is quite insensitive to the absolute size of  $\theta$  just so long as  $0 < \theta \leq 1$ . The definition of  $L(t)$  in (50) is made more precise by characterizing whether or not the animal is awake in terms of the on-cell activity  $x_1(t)$ . We assume that the animal wakes up whenever  $x_1(t)$  exceeds a constant threshold  $C_8$ . Then (50) becomes

$$L(t) = \begin{cases} L^*(t) & \text{if } x_1(t) > C_8 \\ \theta L^*(t) & \text{if } x_1(t) \leq C_8. \end{cases} \quad (51)$$

Figure 4 depicts the case in which  $\theta = 1$ . The case  $\theta = 1$ , however, corresponds to the unphysical assumption that light is equally effective whether or not the animal's eye are closed. When  $\theta$  is chosen less than 1, some subtle but important differences in the phase response curves of nocturnal and diurnal models occur. Figure 5 depicts these phase response curves when  $\theta = 0.1$ . Analogous differences have been reported in

data about nocturnal and diurnal rodents (Pohl, 1982, pp. 341–342). Pohl suggests that these differences have an “important adaptive value” (p. 342). This may indeed be the case, but in our model the differences are due simply to the attenuation of a light pulse when the model animal is asleep.

Pohl describes differences in the phase response curves of nocturnal and diurnal rodents as follows. “In contrast to nocturnal rodents, which are mostly irresponsive to light pulses during rest time (subjective day), the day-active rodents do not show a particular “dead zone” of the PRC” (1982, p. 342). This difference between nocturnal and diurnal animals is explained by our model as follows.

Consider the subjective day of a nocturnal model; that is, the time when the model is asleep (Fig. 5a, left half). When  $\theta=1$  (Fig. 4a), the nocturnal animal is relatively insensitive to a light pulse during the early subjective day because the light pulse excites the off-cells while they are already excited. A small phase advance is nonetheless visible in response to such a pulse. When  $\theta=0.1$  (Fig. 5a), by contrast, hardly any phase shift is evident because the large attenuation of the light pulse occurs at a time when the off-cells are already insensitive to light. When  $\theta=1$  (Fig. 4a), the nocturnal animal is more sensitive to a light pulse during the late subjective day because such a light pulse excites the off-cells while the pacemaker on-cells are becoming active. A significant phase delay therefore occurs. When  $\theta=0.1$  (Fig. 5a), by contrast, the phase delay during the late subjective night is significantly attenuated. The flattening of the phase response curve during the subjective day of a nocturnal model is analogous to the “dead zone” of which Pohl speaks. When the nocturnal model is awake (its subjective night), its phase response curves are the same when  $\theta=1$  (Fig. 4a, right half) and when  $\theta=0.1$  (Fig. 5a, right half).

Similar reasoning explains why the phase response curves of an awake diurnal model are the same whether  $\theta=1$  (Fig. 4b, left half) or  $\theta=0.1$  (Fig. 5b, left half). During the subjective night of a diurnal model, its phase response curve when  $\theta=0.1$  (Fig. 5b, right half) is compressed relative to its phase response curve when  $\theta=1$  (Fig. 4b, right half). Because a diurnal model is asleep while its on-cells are very sensitive to light pulses, the residual phase shift during the subjective night of a diurnal model is greater than the residual phase shift during the subjective day of a nocturnal model. Thus the “adaptive value” of these differences between nocturnal and diurnal animals arise in our model from the simple fact that nocturnal animals go to sleep in response to daylight. These differences can be more quantitatively assessed when more data are collected about how phase response

curves of nocturnal and diurnal animals parametrically depend upon the intensity of light pulses.

## 7 Parametric Structure of Oscillations: Threshold-Linear Signal Function

In this section and the next, we describe how system oscillations depend on choices of the numerical parameters  $C_1, C_2, \dots, C_6$  in Eqs. (5)–(8). We choose both the positive feedback function  $f(w)$  and the negative feedback function  $g(w)$  to be linear above a zero threshold; i.e.,  $f(w)=g(w)=\max(w, 0)$ . In Sect. 9 we show how our conclusions are altered when  $f(w)$  is an S-shaped function. To emphasize properties of endogenous oscillations, we shut the light off ( $L(t)\equiv 0$ ) and observe the model’s free-running behavior in the dark. For all choices of the parameters, the symmetry of Eqs. (5)–(8) during free-run implies that solutions that start out “on the diagonal” remain on the diagonal for all future time. That is, if  $x_1(0)=x_2(0)$  and  $z_1(0)=z_2(0)$ , then  $x_1(t)=x_2(t)$  and  $z_1(t)=z_2(t)$  for all  $t\geq 0$ . The parametric studies reported below illustrate the fact that the diagonal ( $x_1=x_2$  and  $z_1=z_2$ ) is unstable for some, but not all, choices of parameters. In the ensuing discussion, all conclusions are stated for solutions that start off the diagonal:

$$|x_1(0) - x_2(0)| + |z_1(0) - z_2(0)| \neq 0. \quad (52)$$

In this section, we vary each of the parameters  $C_1, C_2, C_3, C_4,$  and  $C_6$  separately while holding all the other parameters fixed at the values given in Table 1. The effects of varying  $C_5$  will be discussed in Sect. 8 because they are qualitatively different from the effects of varying the other five parameters.

Figure 6 and Table 2 depict the effects of varying parameters  $C_1, C_2, C_3, C_4,$  and  $C_6$ . Figure 6 depicts the effects of decreasing the arousal parameter  $C_1$ . In Fig. 6a, a large  $C_1$  value causes the system to approach a “diagonal limit” such that  $x_1(\infty)=x_2(\infty)$  and  $z_1(\infty)=z_2(\infty)$ . This is because the large and equal arousal signals to  $V_1$  and  $V_2$  overcome the influence that the feedback signals  $f(x_1)z_1$  and  $f(x_2)z_2$  can have on system dynamics. As  $C_1$  is parametrically decreased, the system undergoes a bifurcation leading to small amplitude oscillations near the diagonal (Fig. 6b). As  $C_1$  is further decreased, the small amplitude oscillations become large amplitude oscillations (Fig. 6c) that eventually develop a long plateau phase followed by sudden switching between  $x_1$  and  $x_2$  (Fig. 6d). At still smaller  $C_1$  values, all oscillations are quenched, and the system approaches an “off-diagonal limit” (Fig. 6e). That is, one of the potentials wins out over the other potential, in such a way that

$$[x_1(\infty) - x_2(\infty)] [z_1(\infty) - z_2(\infty)] < 0. \quad (53)$$

The choice of initial data determines which potential will win. Oscillations are quenched at small  $C_1$  values for the following reason. Suppose that  $C_1$  is small and that the pair  $(x_1, z_1)$  has the initial advantage over the pair  $(x_2, z_2)$ ; e.g.,  $x_1 > x_2$  and  $z_1 > z_2$ . Then the initially large term  $C_2 f(x_1)z_1$ , which gives positive feedback to  $V_1$ , is never offset by the small arousal  $C_1$  to  $V_2$  as  $z_1$  depletes. That is, although  $z_1$  is eventually depleted by the large signal  $f(x_1)$ , thereby reducing positive feedback from  $V_1$  to itself,  $x_2$  can never recover because its only sources of excitatory input come from its own positive feedback signal, which is small due to  $x_1$ 's initial advantage, and from the small arousal level  $C_1$ . Thus  $x_1$  remains larger than  $x_2$  for all time.

Varying each of the other parameters  $C_2, C_3, C_4$ , and  $C_6$  causes a similar bifurcation series to occur with diagonal and off-diagonal limits flanking out-of-phase oscillations. Table 2 depicts whether an increase or a decrease of a given parameter moves the system from diagonal to off-diagonal limits. An increase in  $C_2$  causes such a transition because it magnifies the positive feedback signals that help  $V_1$  and  $V_2$  dominate each other. An increase in  $C_2$  thus has an effect similar to a decrease in  $C_1$ . An increase in  $C_3$  or  $C_4$  causes similar transitions because it enables a negative feedback signal of fixed size to have a larger inhibitory effect on its target population. The case wherein  $C_4 = 0$  deserves special mention. Then, by Eqs. (5) and (6), no inhibition couples the two-dimensional system  $(x_1, z_1)$  and  $(x_2, z_2)$ . Then, each system  $(x_1, z_1)$  and  $(x_2, z_2)$  approaches a unique limit. Consequently, due to the symmetry of Eqs. (5) and (6) and (7) and (8), the 4-dimensional system (5)–(8) approaches a limit on the diagonal. We emphasize this fact because of its physical importance: inhibitory coupling between on-cells and off-cells is necessary in order for any oscillations to occur. Thus the present model does not take the existence of oscillators for granted and then go on to study how coupling between such oscillators alters their properties, as many contributions based on classical oscillators have done. Instead, we study in detail the mechanisms that generate the oscillatory properties of each pacemaker.

A decrease in  $C_6$  causes a similar oscillation series for a more subtle reason. Large values of  $C_6$  cause both of the positive feedback signals  $f(x_1)z_1$  and  $f(x_2)z_2$  to decay so much that the arousal term  $C_1$  can drive the system to a diagonal limit. Small values of  $C_6$  prevent transmitters from being depleted. Consequently, the transmitters can only accumulate towards their maximal value of 1. Then an initial advantage of (say)  $x_1$  over  $x_2$  tends to be preserved by the large positive feedback signal function  $f(x_1)$ , since  $z_1$  never depletes enough to cause a significant reduction in  $f(x_1)z_1$ .

## 8 Circadian Period and the Transmitter Decay Rate

Parameter  $C_5$  essentially determines the dimensionless period of the freerunning gated oscillator. Figure 7a shows that for sufficiently small  $C_5$ , the period of the oscillation varies linearly with  $C_5^{-1}$ . Thus the slow rate of transmitter accumulation determines a long period of the oscillation.

By contrast with the linear dependence of period on  $C_5^{-1}$ , the model period is insensitive to the choice of the other parameters within a wide range. This important property of our model, which is the basis of its claim to being a "clock", is often assumed as a postulate in other circadian models. Figure 7b illustrates the insensitivity of the period by plotting the period as a function of parameter  $C_1$ . Over most of the parameter range of  $C_1$  values that cause oscillations, the period is approximately constant. At the small  $C_1$  values that border the parameter range giving rise to off-diagonal limits, the period increases rapidly. At the large  $C_1$  values that approach the range of diagonal limits, the period remains approximately constant until  $C_1$  attains a value where the solution bifurcates to diagonal limits.

In summary, given any fixed choice of  $C_5$ , the period of the oscillator is essentially determined no matter how the other parameters are chosen, except near the limiting parametric values where the oscillation is quenched.

An increase of  $C_5$  from zero causes the following sequence of solutions to occur. When  $C_5 = 0$ ,  $z_1$  and  $z_2$  are constant by (7) and (8). The system approaches off-diagonal limits except possibly when  $z_1 = z_2$ . As soon as  $C_5 > 0$ , large amplitude oscillations occur. At sufficiently large  $C_5$  values, diagonal limits occur.

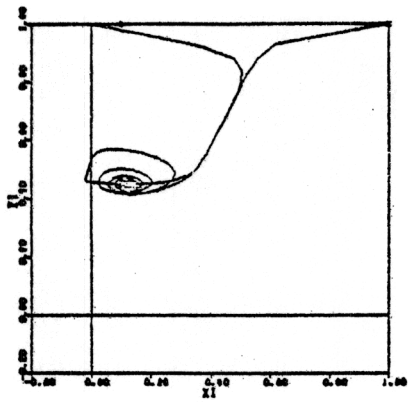
## 9 Dependence of Solution Types on Signal Function: The Sigmoid Case

All of the above properties hold when the positive feedback signal  $f(w)$  and the negative feedback signal  $g(w)$  equal a threshold-linear signal function  $\max(w, 0)$ . When  $f(w)$  is chosen instead to be the sigmoid function

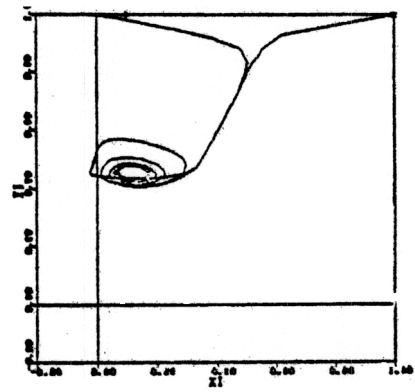
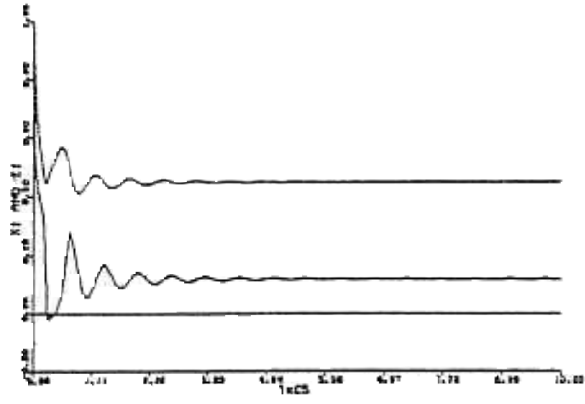
$$f(w) = \begin{cases} \frac{w^2}{C_7^2 + w^2} & \text{if } w \geq 0 \\ 0 & \text{if } w < 0, \end{cases} \quad (25)$$

then a much richer family of solution types can occur.

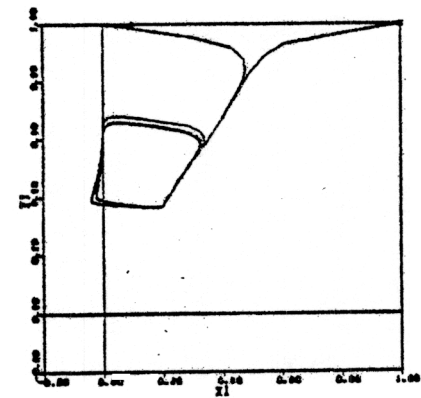
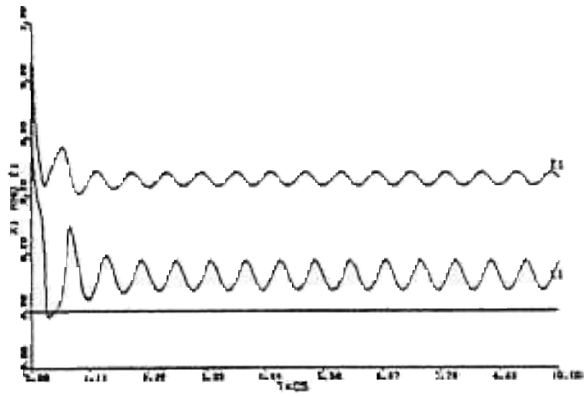
Sigmoid signal functions play an important role in competitive feedback networks whose feedback signals are not modulated by slow gates. In such networks, the sigmoid signal function attenuates small activities (noise suppression) and amplifies large activities (con-



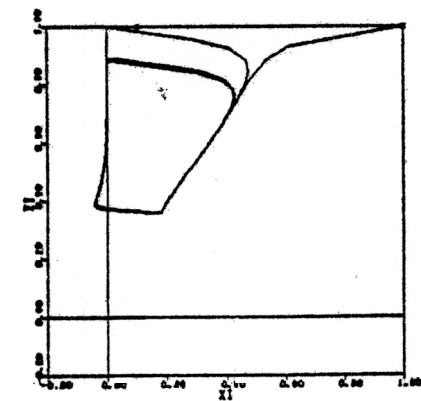
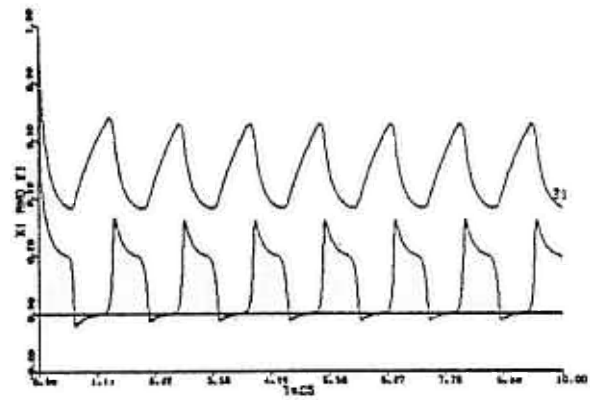
a



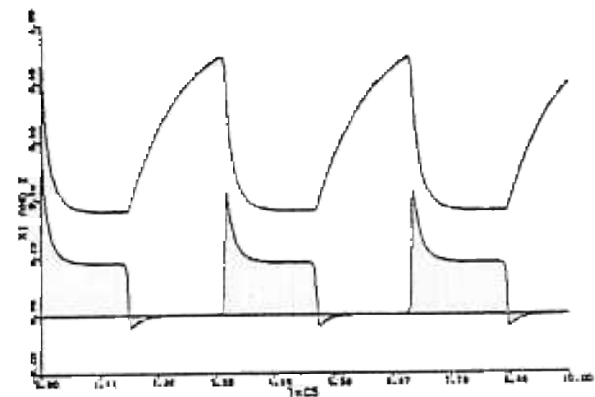
b



c



d



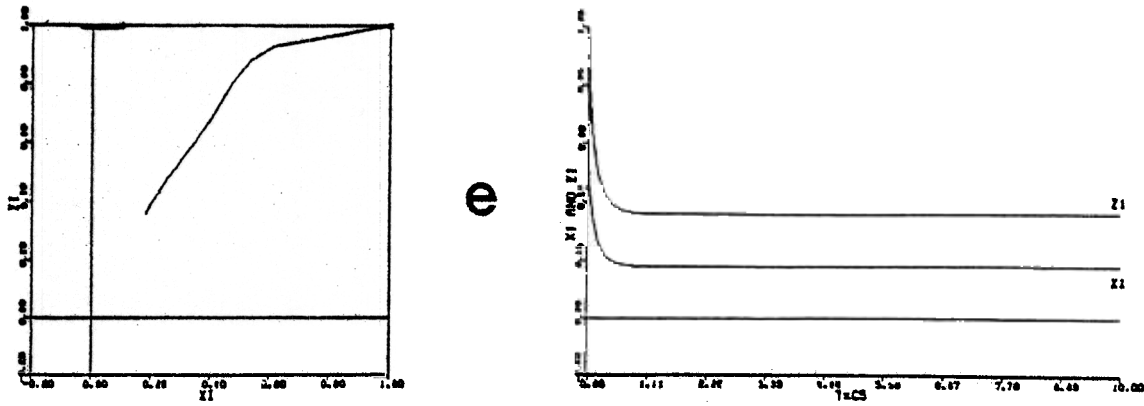


Fig. 6a-e. Oscillation sequence in response to a decrease in dimensionless arousal  $C_1$  (threshold-linear case). a Diagonal limits ( $C_1=0.18$ ). b Small amplitude oscillation ( $C_1=0.17$ ). c Large amplitude oscillation ( $C_1=0.1$ ; Table 1). d Plateau oscillation ( $C_1=0.0895$ ). e Off-diagonal limit ( $C_1=0.0893$ ). The same time scale is used on all the graphs

Table 2. Oscillation sequences due to individual parametric variations ( $C_5 = 0.01$ ; threshold-linear case)

a	b	c	d	e
Limit on the diagonal: $x_1 = x_2$ and $z_1 = z_2$	Small amplitude oscillations near the diagonal	Large amplitude oscillations, with $C_1 \dots C_6$ as in Table 1	Large amplitude oscillations with long plateau	Limit off the diagonal $x_1$ wins or $x_2$ wins
Large $C_1$ : $C_1 > 0.177$	→ decreasing $C_1$	$C_1 = 0.1$		Small $C_1$ : $0.0895 > C_1$
Small $C_2$ : $C_2 < 1.28$	→ increasing $C_2$	$C_2 = 2$		Large $C_2$ : $2.24 < C_2$
Small $C_3$ : $C_3 < 0.062$	→ increasing $C_3$	$C_3 = 0.1$		Large $C_3$ : $0.106 < C_3$
Small $C_4$ : $C_4 < 3.46$	→ increasing $C_4$	$C_4 = 5$		Large $C_4$ : $5.34 < C_4$
Large $C_6$ : $C_6 > 23.0$	→ decreasing $C_6$	$C_6 = 10$		Small $C_6$ : $8.34 > C_6$

trast enhancement) before storing the contrast enhanced activity pattern in short term memory via feedback (Grossberg, 1982b). When slow gates can modulate sigmoid feedback signals, as in a gated pacemaker, then the storage process is replaced by a wide variety of oscillatory possibilities.

Sigmoid signal functions also have a simple physical interpretation that is of independent interest. Suppose that  $f(w)$  is the total output of a large population of cells. Let each cell fire a signal of unit intensity when its activity exceeds a threshold  $\Gamma$ ; otherwise let the cell output equal zero. Suppose that the number  $p(\Gamma)$  of cells having a fixed threshold  $\Gamma$  is a bell-shaped function of  $\Gamma$ . Then

$$f(w) = \int_0^w p(\Gamma) d\Gamma \quad (54)$$

is a sigmoid function of  $w$ . Thus if the signal thresholds of a cell population are randomly distributed about a

mean threshold value, then the total population signal is a sigmoid function of its mean activity.

In the following examples, the nonlinear curvature of  $f(w)$  causes the new oscillatory types, rather than a rescaling of numerical parameters. This claim is illustrated in Fig. 8, which graphs the previous choice of threshold-linear signal function and the present choice of sigmoid signal function. In the threshold-linear case, we chose  $C_2 = 2$  so that  $C_2 f(w) = 2w$  when  $w \geq 0$ . In the sigmoid case, we choose  $C_2 = 1$  and  $C_7 = 0.2$ , so that

$$C_2 f(w) = \frac{w^2}{0.04 + w^2} \quad (55)$$

if  $w \geq 0$ , which remains very close to  $2w$  throughout the interval  $[0, 0.4]$  wherein the graphs of  $x_1(t)$  and  $x_2(t)$  are concentrated. Note that at very small values of  $w \in [0, 0.4]$ , the sigmoid signal is smaller than  $2w$ , whereas at larger values of  $w \in [0, 0.4]$ , the sigmoid

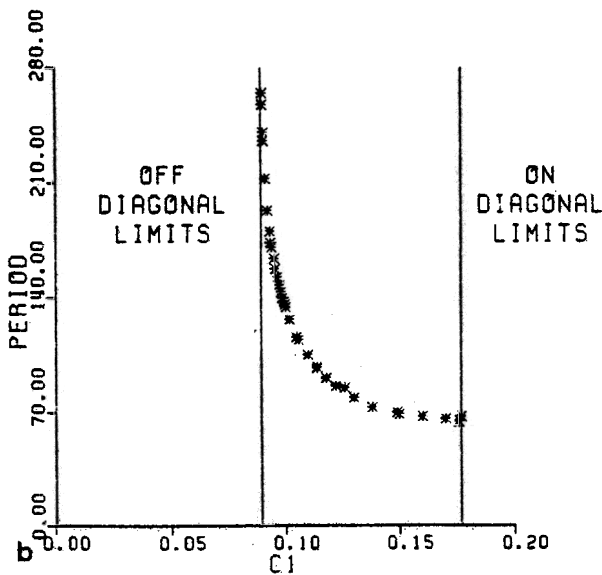
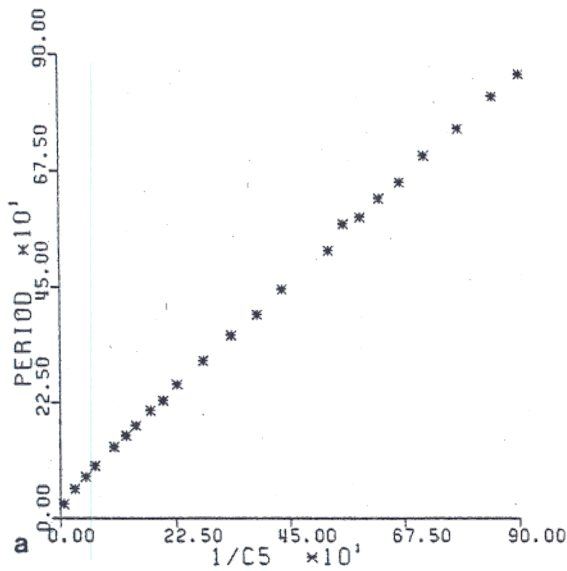


Fig. 7a and b. Circadian period (threshold-linear case). a For small values of the dimensionless transmitter accumulation rate  $C_5$ , the period varies linearly with  $C_5^{-1}$ . When  $C_5 > 0.143$ , the system goes to diagonal limits. b The period is relatively insensitive to the dimensionless arousal level  $C_1$  except near its extreme values where oscillations break down

signal exceeds  $2w$ . Thus  $2w$  closely interpolates the sigmoid signal throughout the interval of interest. In particular, we choose  $C_7 = 0.2$  so that  $w^2 / (C_7^2 + w^2) = \frac{1}{2}$  when  $w = 0.2$ . Thus the sigmoid signal function attains half its maximum value at the estimated average value 0.2 of  $x_1$  and  $x_2$ . Table 3 summarizes the choice of parameters off which we will perturb to study the sigmoid case. Parameters  $C_1$ ,  $C_3$ ,  $C_4$ ,  $C_5$ , and  $C_6$  have the same values as in Table 1, and parameters  $C_2$  and  $C_7$  are chosen so that the sigmoid function interpolates the threshold-linear function.

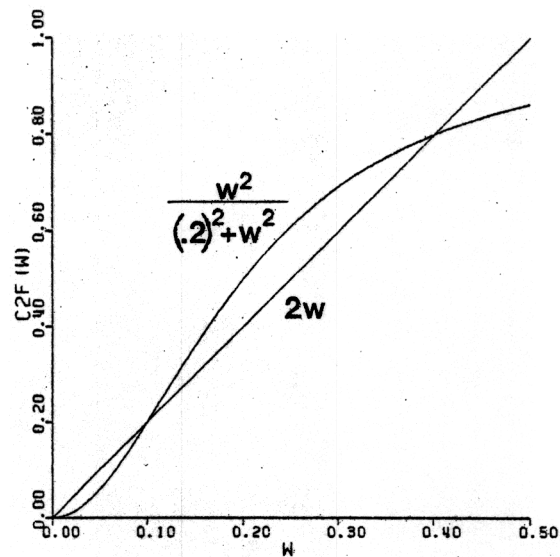


Fig. 8. Interpolated sigmoid and threshold-linear signal functions. The parameters  $C_2 = 1$  and  $C_7 = 0.2$  are chosen so that the sigmoid signal function closely interpolates the threshold-linear function ( $C_2 = 2$ ) throughout the range of oscillations

Table 3. Typical parameter values for a sigmoid nocturnal pacemaker

$C_1 =$	0.10
$C_2 =$	1.00
$C_3 =$	0.10
$C_4 =$	5.00
$C_5 =$	0.01
$C_6 =$	10.00
$C_7 =$	0.20

## 10 Parametric Structure of Oscillations: Sigmoid Signal Function

In this section, we will summarize the oscillation sequences that can occur when the parameters  $C_1$ ,  $C_2$ ,  $C_3$ ,  $C_4$ , and  $C_6$  are separately varied. The next section will consider the remarkable oscillation sequences that can occur when  $C_7$  is varied. These new sequences can also occur when any one of the other parameters is varied, albeit in a region of parameter space other than that summarized in Table 3.

A decrease in the arousal parameter  $C_1$  generates an oscillation sequence much like that described in Sect. 7 and illustrated in Fig. 6, with one notable exception. In Sect. 7, a decrease in  $C_1$  transformed large amplitude oscillations into plateau oscillations in which  $x_1$  and  $x_2$  overshoot and then decreased to a plateau level before being inhibited (Fig. 6d). As  $C_1$  decreased in this parameter range, the period of the oscillation increased continuously (Fig. 7b). By contrast, in the sigmoid case, a decrease of  $C_1$  transforms a

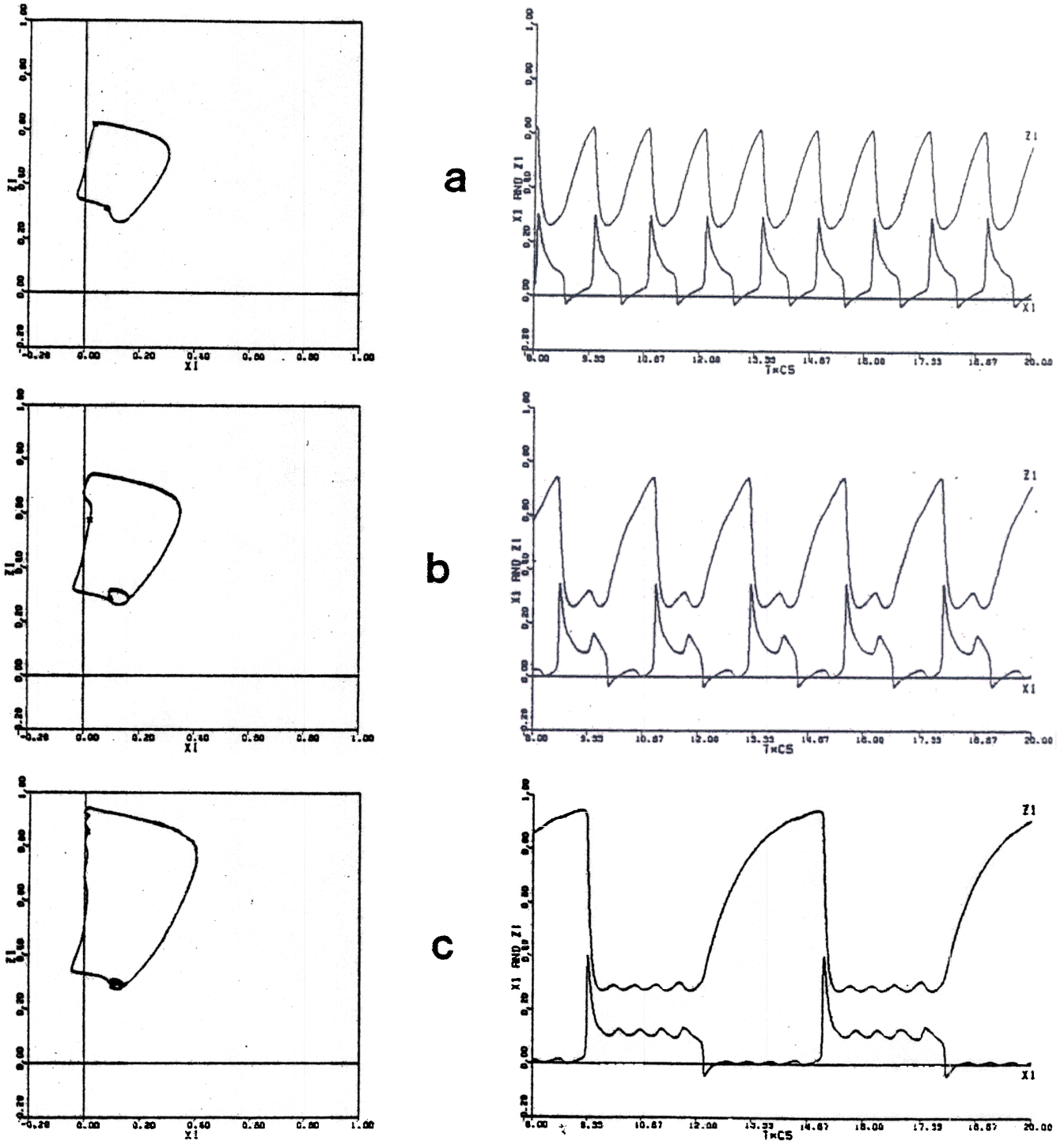


Fig. 9a–c. Rippled plateau solutions in response to a decrease in dimensionless arousal  $C_1$  (sigmoid case). a At  $C_1 = 0.076048$ , a large amplitude oscillation occurs. b At  $C_1 = 0.076047$ , a second bump occurs during each cycle. c At  $C_1 = 0.066$ , the plateau contains four ripples. At slightly smaller  $C_1$  values, off-diagonal limits occur

large amplitude oscillation (Fig. 9a) into an oscillation in which a second bump occurs in the graphs of  $x_1$  and  $x_2$  instead of a smooth plateau (Fig. 9b). As this bump appears, a discontinuous increase of the period also occurs. A further decrease of  $C_1$  eventually causes a

second, then a third, etc., bump to occur in the graphs of  $x_1$  and  $x_2$  (Fig. 9c). Each new bump is accompanied by a discontinuous increase of the period. At sufficiently small values of  $C_1$ , these oscillations are replaced by off-diagonal limits, as in the threshold-

linear case. These *rippled plateau* solutions have never been observed during our numerical studies of the threshold-linear case and are thus presumably due to the nonlinear form of the sigmoid signal function.

Changing each of the parameters  $C_2, C_3, C_4,$  and  $C_6$  in the direction described in Table 2, while holding the other parameters at their values in Table 3, also generates the sequence of diagonal limits, small amplitude oscillations, large amplitude oscillations, rippled plateau oscillations, and off-diagonal limits.

### 11 Mittens, Oyster Shells, Sequence Clusters, and Chaos

When  $C_7$  is increased with the parameters  $C_1, \dots, C_6$  fixed at their values in Table 3, then the following type of oscillation sequence is observed:

- diagonal limits
- large amplitude, small period oscillations

- larger amplitude oscillations, monotone increase in period
- smaller amplitude oscillations, levelling off of period
- mittens (period doubling)
- oyster shells (slowly modulated mittens)
- sequence clusters (periodic sequences of oscillation clusters)
- complex transitions, chaos?
- unstable small amplitude oyster shells
- diagonal limits.

Figure 10 illustrates these solution types.

The diagonal limits (Fig. 10a) that are found when  $C_7$  is very small are due to the fact that the positive feedback signals  $f(x_1)$  and  $f(x_2)$  are approximately equal and constant in this range. The large amplitude oscillations (Fig. 10b) that occur at slightly larger  $C_7$  values are due to the fact that  $f(w)$  approximates a step function with a transition from approximately 0 to 1 as

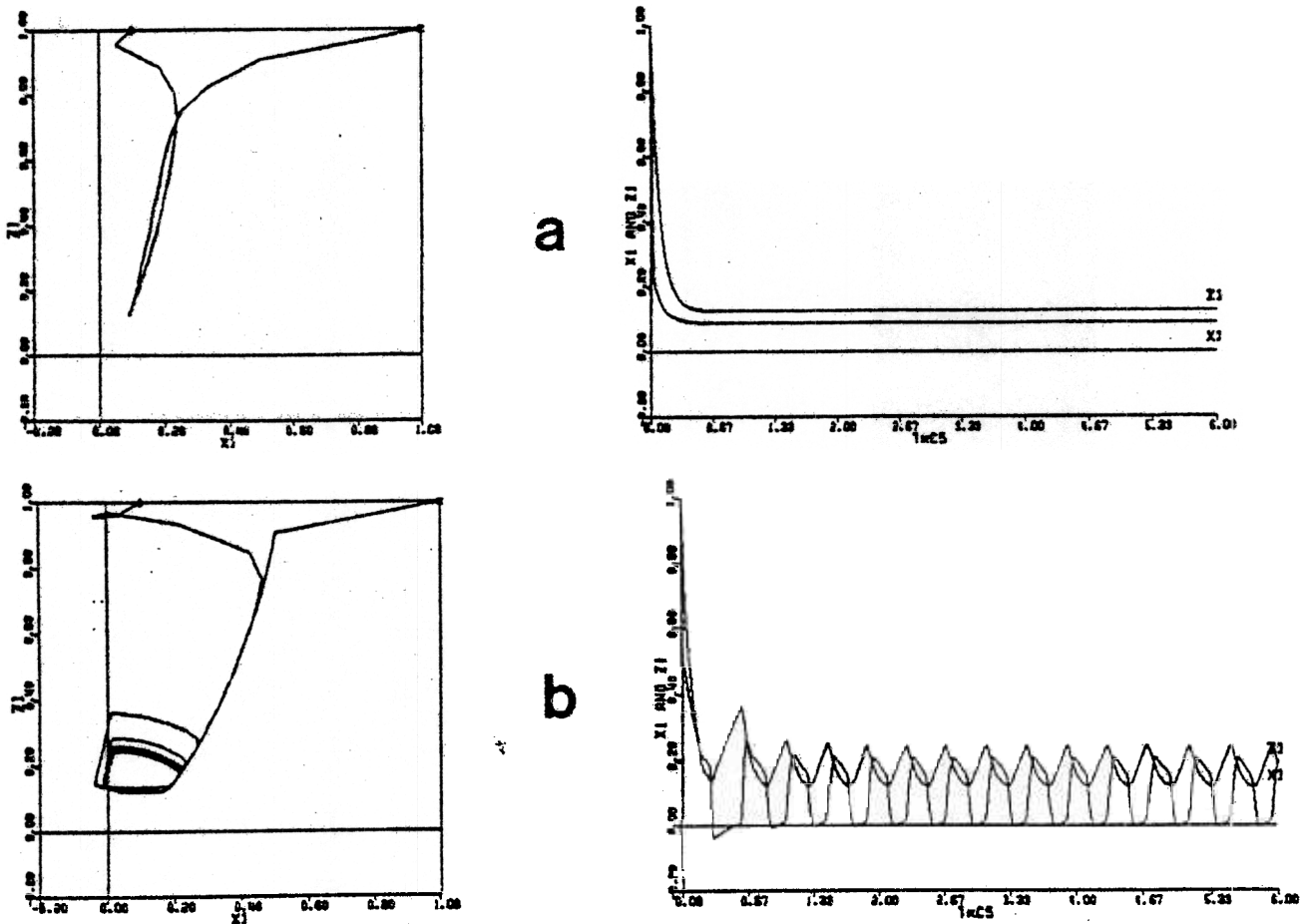
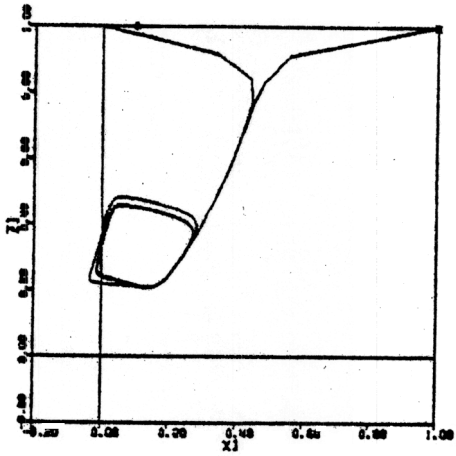
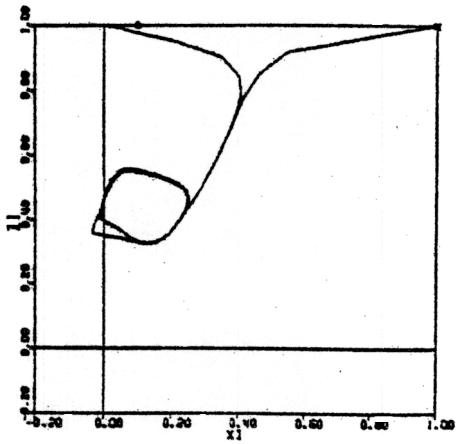
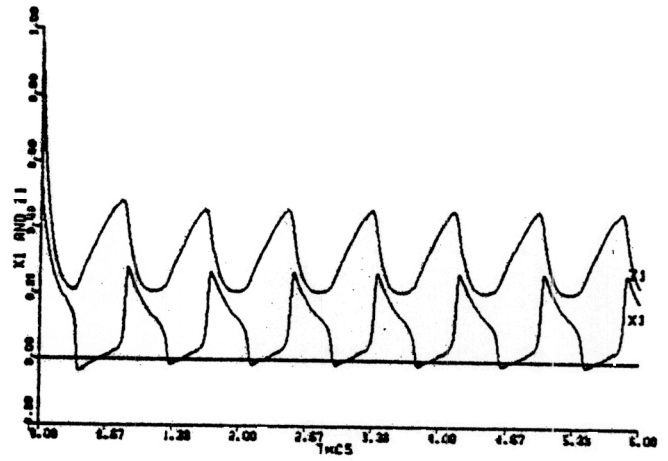


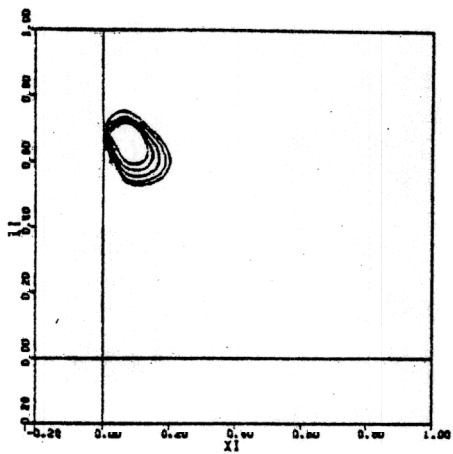
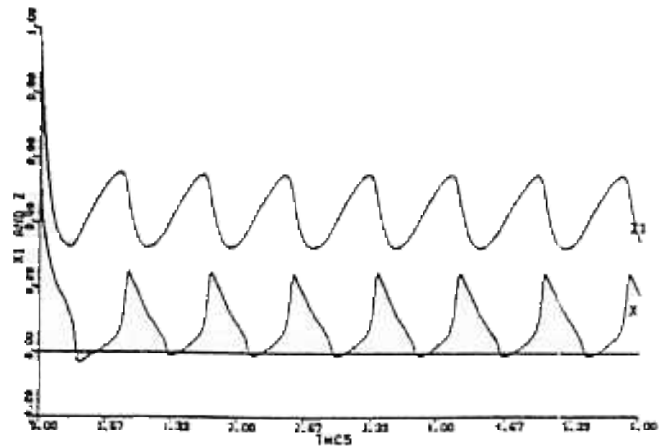
Fig. 10a-j. Oscillation sequence in response to an increase in the half-maximum argument  $w = C_7$  of the sigmoid signal  $f(w)$ . a Diagonal limit ( $C_7 = 0.0577$ ). b Fast large amplitude oscillation ( $C_7 = 0.0578$ ). In this case, the values of  $z_1$  are so small that the graphs of  $x_1(t)$  and  $z_1(t)$  intersect. c Longer period and larger amplitude oscillation ( $C_7 = 0.17$ ). d Smaller amplitude oscillation and same period as in c ( $C_7 = 0.25$ ). e Mittens ( $C_7 = 0.348$ ). f Oyster shells ( $C_7 = 0.35$ ). g (8, 5, 5) sequence cluster ( $C_7 = 0.36$ ). h Triplets ( $C_7 = 0.363$ ). i Unstable small amplitude oyster shells become regular periodic ( $C_7 = 0.368$ ). j Diagonal limit ( $C_7 = 0.375$ ). The phase portraits have been enlarged in f and g



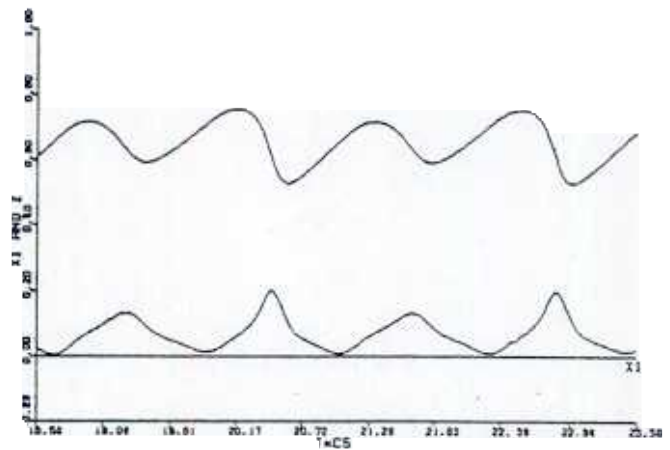
c

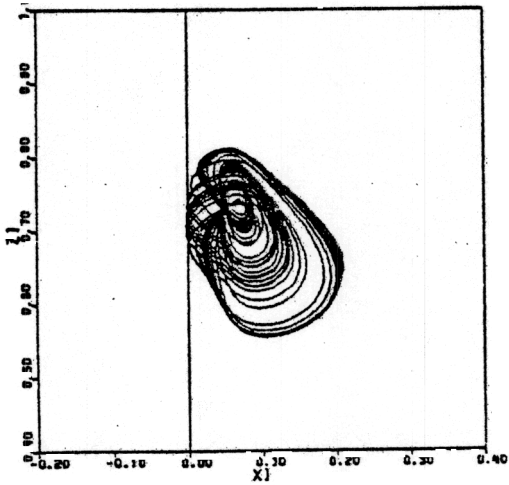
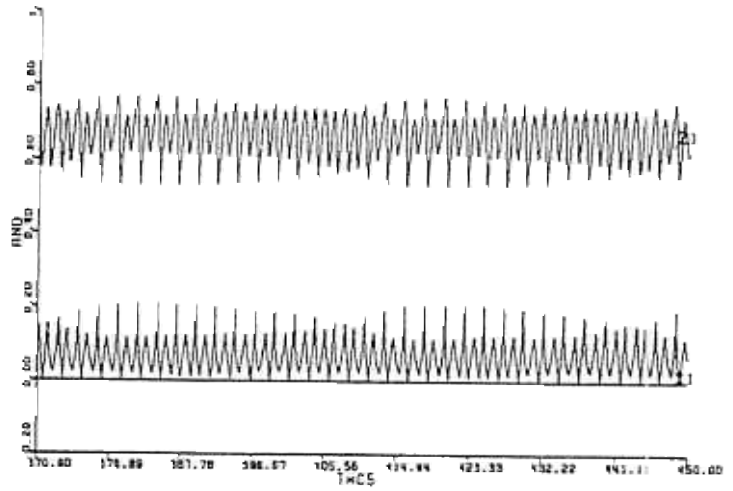
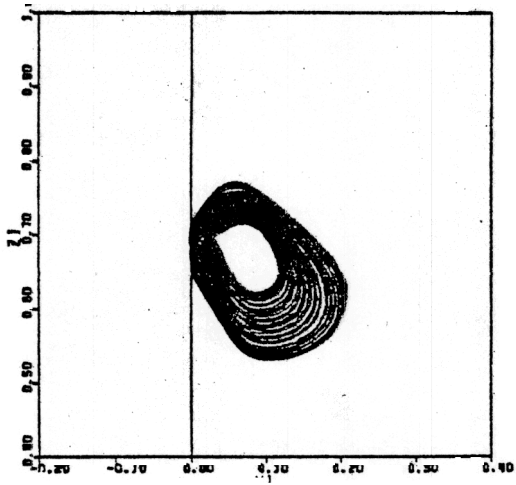


d

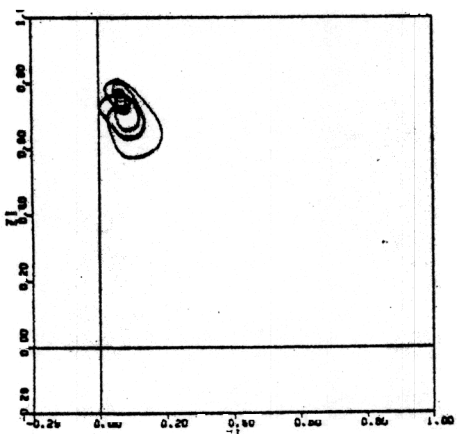
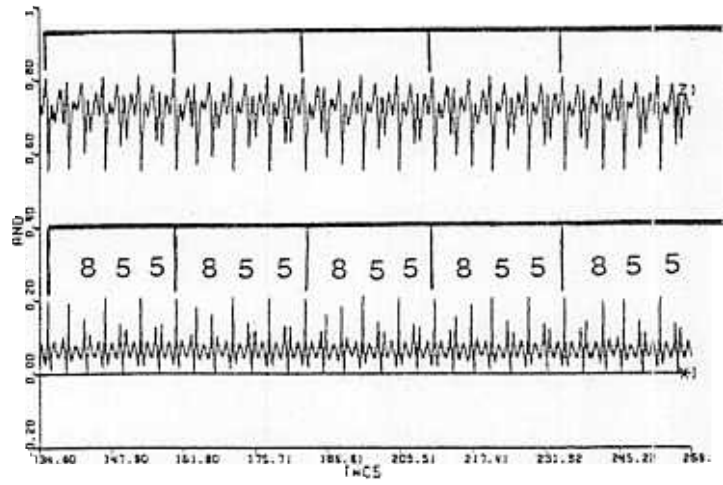


e

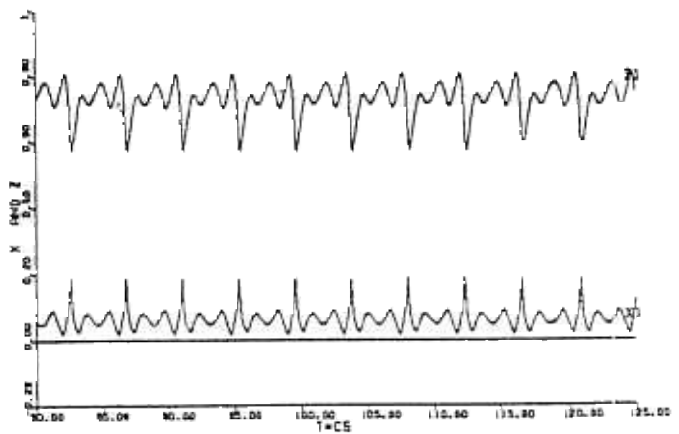


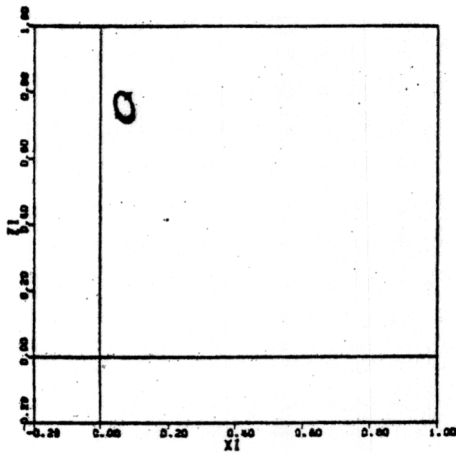


g

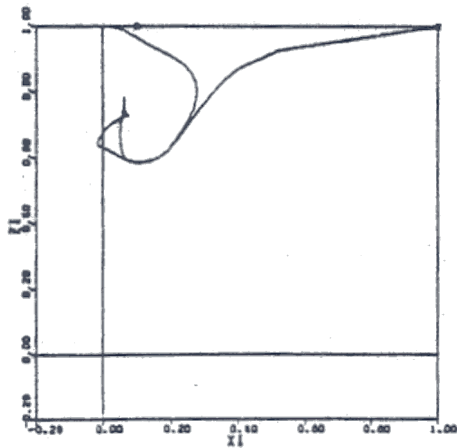
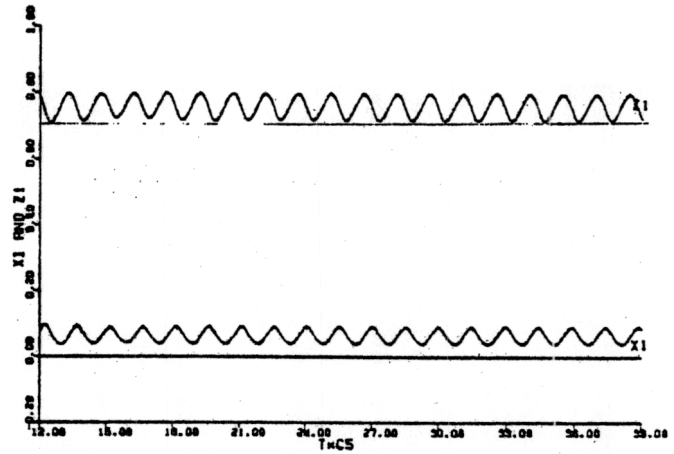


h

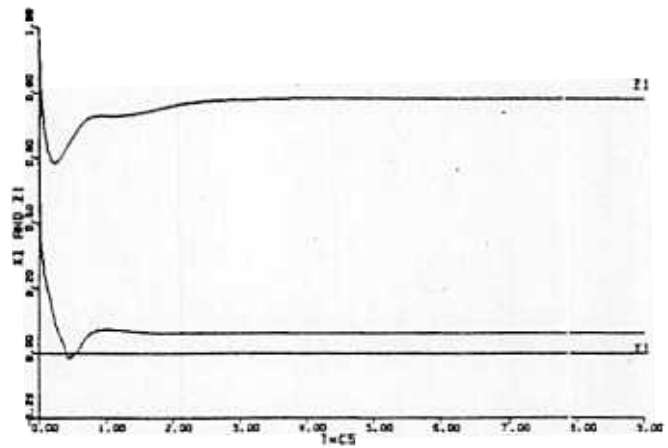




i



j



$w$  exceeds  $C_7$  (Fig. 11a). The longer periods of large amplitude oscillations (Fig. 10c) that are found at larger  $C_7$  values (Fig. 11b) can be explained as follows. The reversal of the relative sizes of  $x_1$  and  $x_2$  occurs relatively quickly. This reversal is called a *jump* in the terminology of singular perturbation theory (Sect. 12). At larger values of  $C_7$ , the maximal difference between  $x_1$  and  $x_2$  is also larger. Hence  $z_1$  and  $z_2$ , which change slowly (Sect. 8), take longer to equilibrate to the  $x_1$  and  $x_2$  values. In the terminology of singular perturbation theory, this slow process is said to take place on the *slow manifold* (Sect. 12). The longer duration of the slow manifold process is the major factor determining how the period can increase with  $C_7$ .

As  $C_7$  increases further, one might expect, as in Sect. 7, that small amplitude oscillations will be generated, because an increase in  $C_7$  acts in much the same way as an increase in  $C_1$  or a decrease in  $C_2$  (Fig. 11a). However, this is not all that happens. The amplitude of oscillations does begin to decrease as the period levels off (Figs. 10d and 11b). As  $C_7$  increases further, however, period doubling occurs (Fig. 10e) due to the

attenuation of alternate peaks in the graphs of each  $x_i$  and  $z_i$ ,  $i=1, 2$  ("mittens"). When this occurs, the largest peaks and troughs of  $x_1(t)$  are aligned with the largest troughs and peaks of  $x_2(t)$ , respectively. Consequently the graphs of  $x_1(t)$  and  $x_2(t)$  are out of phase, but no longer  $180^\circ$  out of phase.

At larger  $C_7$  values, the envelopes of the mittens are modulated on a slow time scale (Fig. 10f). We call this oscillation type an *oyster shell* due to the appearance of its  $(x_1, z_1)$  phase portrait. A striking feature of the oyster shell is that a periodic modulation of the envelope of oscillation peaks coexists with a periodic modulation of the envelope of oscillation troughs. This type of envelope modulation differs, say, from the modulation that occurs during the beats of a harmonic oscillator, where the peaks and troughs share a common envelope.

At larger  $C_7$  values, periodic sequences of oscillation clusters appear. Figure 10g depicts an oscillation in which a cluster of eight peaks is followed by two repetitions of a different cluster of five peaks, after which the (8, 5, 5) sequence repeats itself. Interspersed

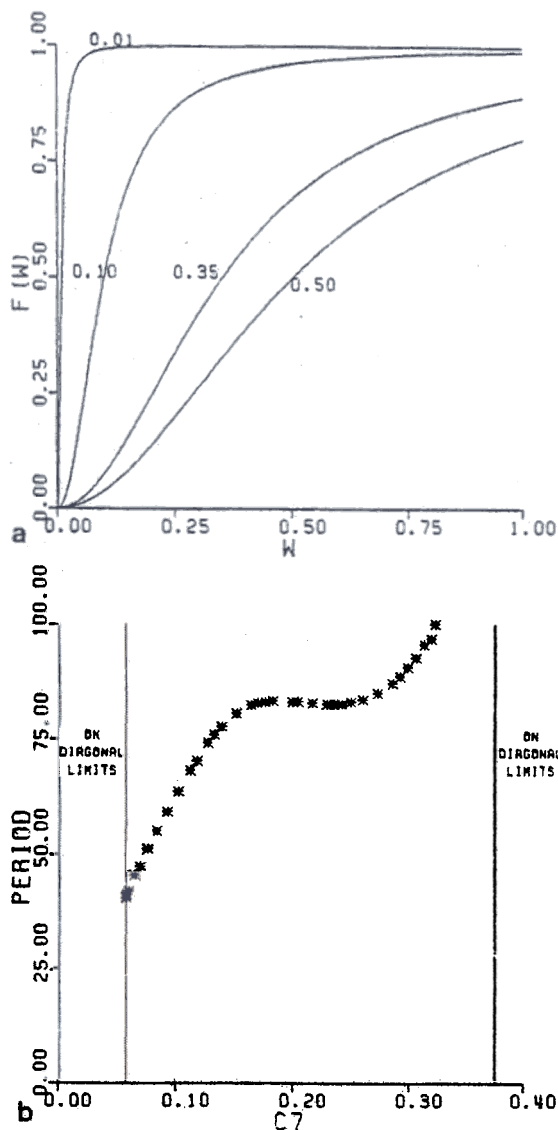


Fig. 11a and b. Dependence of sigmoid signal function and oscillation period on  $C_7$ . a A family of sigmoid signal functions parameterized by  $C_7$ . b Period as a function of  $C_7$ . Note the constancy of the period except where the sigmoid approximates a 0-1 switch (small  $C_7$ ) or near where complex oscillations occur (large  $C_7$ )

among the modulated solutions are relatively simple patterns, such as the unmodulated triplets depicted in Fig. 10h. This complex sequence of patterns suggests that chaotic solutions may be present for some  $C_7$  values.

Only after these complex waveforms are generated does the system experience a progressive decrease in the amplitude of oyster shells (Fig. 10i). Figure 10i indicates that the small amplitude oyster shell is unstable, since the solution eventually approaches a small amplitude regular periodic solution. At still larger  $C_7$  values, diagonal limits are obtained. The diagonal limits occur because a sufficient attenuation

of  $f(w)$  acts much like a large  $C_1$  or small  $C_2$  value (Sect. 7).

Why does a series of complex oscillation types occur instead of just a steady reduction in the amplitude of a regular periodic solution, as when  $f(w)$  is a threshold-linear signal function (Sect. 7)? A mathematical explanation of this phenomenon is not yet available, but the following facts indicate that the quadratic nonlinearity in  $f(w)$  at small  $w$  values causes the phenomenon.

In all of our numerical studies of these oscillations,  $x_1(t)$  and  $x_2(t)$  remain smaller than  $C_7$  at all times  $t \geq 0$ . Within this range of values,  $f(w)$  is well approximated by  $w^2/C_7^2$ . To test whether a quadratically nonlinear signal function can generate Fig. 10a-j, we replaced the sigmoid  $f(w)$  by  $w^2/C_7^2$  and verified that a complex oscillation sequence was in fact generated using this quadratic signal function.

An indication of how mittens (Fig. 10e) and the modulated mittens, or oyster shells (Fig. 10f), may be generated is contained in the following intuitive argument. Mittens consist of small amplitude peaks that alternate with large amplitude peaks. The large amplitude peaks are analogous to the large amplitude peaks of a regular periodic solution (Fig. 10d). Our problem is to understand why the smaller peaks are not full size. Consider the time  $t = \alpha$  in Fig. 12a at which  $x_1(t)$  attains a minimum. At this time,  $x_1$  and  $x_2$  begin to switch because  $z_2$  is sufficiently depleted to make

$$(1 - x_1)(C_1 + C_2 f(x_1)z_1) > (1 - x_2)(C_1 + C_2 f(x_2)z_2) \quad (56)$$

despite the fact that  $f(x_1) \cong 0$  (Sect. 3). Consequently  $x_1$  begins to grow. A complete switch from  $x_2$  to  $x_1$  is caused when, as  $x_1$  grows, also  $f(x_1)z_1$  grows sufficiently quickly to support this regenerative reaction. Figure 12b indicates, however, that when  $x_1$  is in this range of values, and numerically approximates 0.1, the value of  $x_1^2/C_7^2$  is very small. By "very small", we mean small compared to a linear signal function  $1.3x_1$  at which small amplitude, regular periodic oscillations are found (Table 2). The insufficient positive feedback from  $x_1^2/C_7^2$  prevents  $x_1$  from completing a full switch with  $x_2$ .

Due to  $x_1$ 's partial growth,  $z_1$  continues to deplete, thereby causing a decrease in  $f(x_1)z_1$  that accompanies a decrease in  $x_1$  between times  $t = \beta$  and  $t = \gamma$ . During these times,  $z_1$  attains an intermediate set of values, neither maximal nor minimal, because  $x_1$  itself has not reached its extrema. As  $x_1$  continues to decrease,  $z_1$  begins to accumulate again, this time starting from a larger initial value than is attained at time  $t = \alpha$ . Thus when the next opportunity for switching between  $x_1$  and  $x_2$  occurs at time  $t = \gamma$ ,  $f(x_1)z_1$  is bolstered by a large  $z_1$  value. This boost enables  $x_1$  to move towards

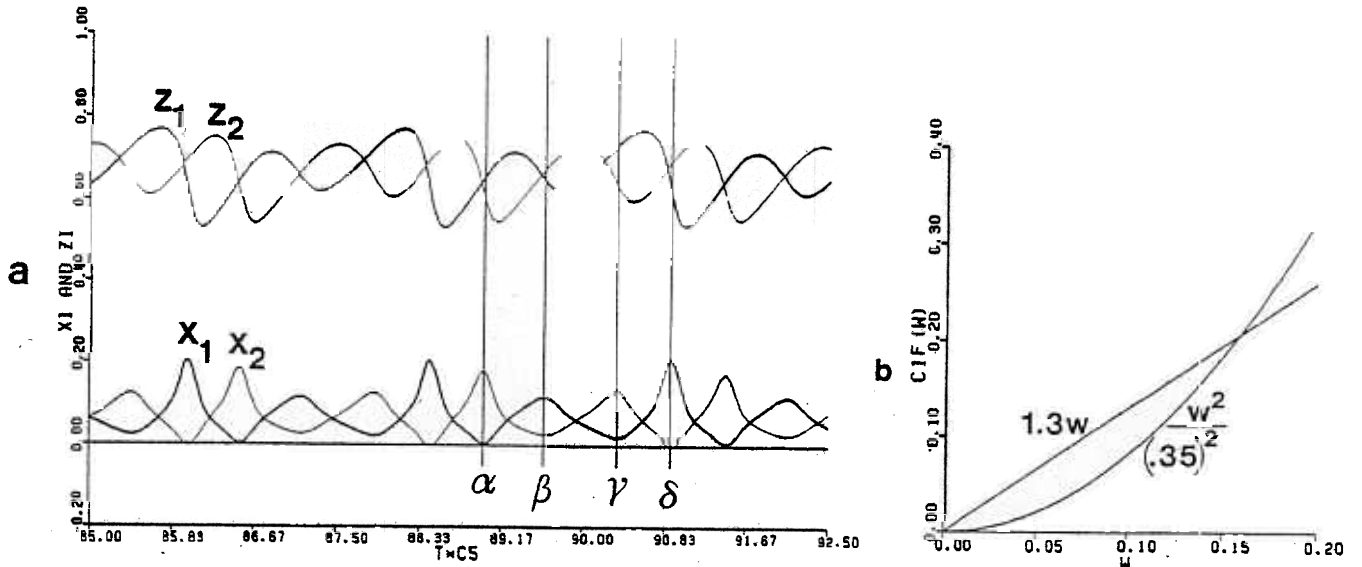


Fig. 12a and b. Dependence of mittens on quadratic growth of the sigmoid signal. **a** Graphs of  $x_1(t)$  and  $z_1(t)$  (dark curves) and  $x_2(t)$  and  $z_2(t)$  (light curves). Text describes how lower peaks in  $x_1$ 's graph are caused by insufficient quadratic feedback. Here,  $C_7 = 0.35$ , as in Fig. 10f. **b** When  $w = 0.1$ ,  $w^2/(0.35)^2 < 1.3w$ . By contrast, when  $w = 0.2$ ,  $w^2/(0.35)^2 > 1.3w$ . The different relative sizes of quadratic vs. linear feedback signals control whether mittens or a small amplitude, regular periodic solution occurs

a value of approximately 0.2. By Fig. 12b,  $x_1^2/C_7^2$  is much larger when  $x_1 = 0.2$  than is the comparison linear signal function  $1.3x_1$ . Thus a better switch between  $x_1$  and  $x_2$  is assured than in the threshold-linear case, where small amplitude oscillations occurred.

## 12 Singular Perturbation Analysis

This section outlines a singular perturbation analysis of how a gated pacemaker oscillates. The analysis can be expanded into a formal proof using known techniques for building isolating blocks in four-dimensional fast-slow dynamical systems (Carpenter, 1977a, b). The discussion will focus on system (5)–(8) when  $f(w) = g(w) = \max(w, 0)$  and  $L(t) \equiv 0$  (free-run). We consider this system in the singular limit where  $C_5$  is very small. Then  $z_1$  and  $z_2$  change very slowly compared to  $x_1$  and  $x_2$  except near the set  $\mathcal{S}$  where both  $\dot{x}_1 = 0$  and  $\dot{x}_2 = 0$ . The set

$$\mathcal{S} = \{(x_1, x_2, z_1, z_2) : \dot{x}_1 = 0 \text{ and } \dot{x}_2 = 0\} \quad (57)$$

is called the *slow manifold* of the system. Off the set  $\mathcal{S}$ ,  $z_1$  and  $z_2$  can be approximated by constants along system trajectories. Then the four-dimensional system (5)–(8) is approximately described by the two-dimensional *fast system*  $\mathcal{F}$

$$\begin{aligned} \dot{x}_1 &= -x_1 + (1 - x_1)[C_1 + C_2 f(x_1)z_1] \\ &\quad - (x_1 + C_3)C_4 g(x_2) \end{aligned} \quad (58)$$

and

$$\begin{aligned} \dot{x}_2 &= -x_2 + (1 - x_2)[C_1 + C_2 f(x_2)z_2] \\ &\quad - (x_2 + C_3)C_4 g(x_1) \end{aligned} \quad (59)$$

in which  $z_1$  and  $z_2$  are constant. The fast system (58) and (59) can be rewritten in the form

$$\dot{y}_1 = a_1(y_1)[b_1(y_1) - c(y_1, y_2)] \quad (60)$$

and

$$\dot{y}_2 = a_2(y_2)[b_2(y_2) - c(y_1, y_2)] \quad (61)$$

in terms of the variables  $y_i = x_i + C_3$ ,  $i = 1, 2$ .

When a competitive system has this form, it is called an *adaptation level system*. Adaptation level systems have the property that all their trajectories are attracted to equilibrium points (Grossberg, 1978, 1982b). Consequently, the trajectory approaches the slow manifold  $\mathcal{S}$ . When this occurs,  $\dot{x}_1 \cong 0$  and  $\dot{x}_2 \cong 0$  so that even if  $C_5$  is small, the rates of change of  $z_1$  and  $z_2$  become significant. Then the motions of  $z_1$  and  $z_2$  are studied while the trajectory remains on  $\mathcal{S}$ . In other words, we consider equations

$$\dot{z}_1 = C_5[1 - z_1 - C_6 f(x_1)z_1] \quad (7)$$

and

$$\dot{z}_2 = C_5[1 - z_2 - C_6 f(x_2)z_2] \quad (8)$$

given the hypothesis that  $x_1$  and  $x_2$  satisfy the simultaneous equations

$$\begin{aligned} 0 &= -x_1 + (1 - x_1)[C_1 + C_2 f(x_1)z_1] \\ &\quad - (x_1 + C_3)C_4 g(x_2) \end{aligned} \quad (62)$$

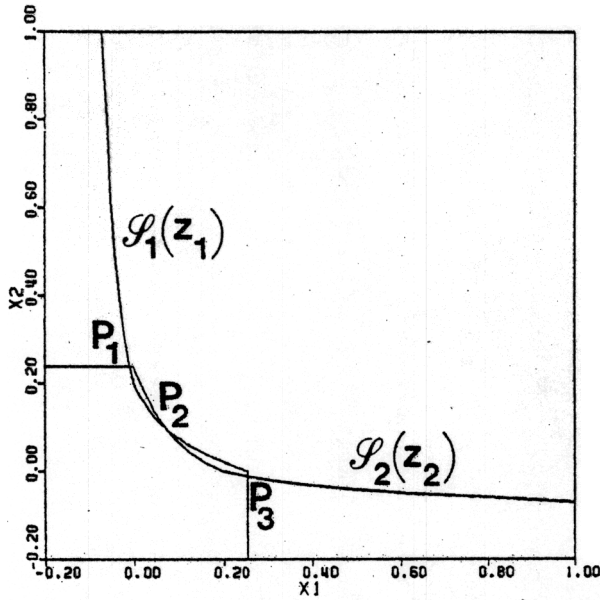


Fig. 13. Fast manifold and its equilibrium points  $P_1$ ,  $P_2$ , and  $P_3$  (threshold-linear case). Parameters  $C_1$ ,  $C_2$ ,  $C_3$ , and  $C_4$  are chosen as in Table 1. Parameter  $z_1=0.473$  and  $z_2=0.448$ . Sets  $\mathcal{S}_1(z_1)$  and  $\mathcal{S}_2(z_2)$  are defined in the text

and

$$0 = -x_2 + (1-x_2)[C_1 + C_2 f(x_2)z_2] - (x_2 + C_3)C_4 g(x_1). \quad (63)$$

In this case,  $x_1$  and  $x_2$  satisfy equations of the form

$$x_1 = h_1(z_1, z_2) \quad (64)$$

and

$$x_2 = h_2(z_1, z_2) \quad (65)$$

which represent a single-valued branch of the solution of (62) and (63). Then (7) and (8) become

$$\dot{z}_1 = C_5[1 - z_1 - C_6 f(h_1(z_1, z_2))z_1] \quad (66)$$

and

$$\dot{z}_2 = C_5[1 - z_2 - C_6 f(h_2(z_1, z_2))z_2]. \quad (67)$$

This two-dimensional system determines the motion of  $(z_1, z_2)$  unless a phase point is reached at which a solution  $(x_1, x_2)$  of (66) and (67) no longer exists on  $\mathcal{S}$ . At such a time, the trajectory jumps off  $\mathcal{S}$ . Then  $\mathcal{F}$  controls system dynamics until  $x_1$  and  $x_2$  approach  $\mathcal{S}$  once again.

A singular solution of the system is constructed from alternating solution segments on  $\mathcal{F}$ ,  $\mathcal{S}$ ,  $\mathcal{F}$ ,  $\mathcal{S}$ , .... Singular perturbation techniques can be used to show that solutions of the full system exist close to a singular solution when  $C_5$  is very small. The following description indicates how the phase portraits of  $\mathcal{F}$  and  $\mathcal{S}$  can generate a singular periodic solution.

Suppose for definiteness that the trajectory is not in  $\mathcal{S}$  at time  $t=0$ . Figure 13 indicates how the trajectory moves in  $\mathcal{F}$ . Figure 13 is an  $(x_1, x_2)$  phase portrait in which two curves intersect. One curve describes the set

$$\mathcal{S}_1(z_1) = \{(x_1, x_2) : \dot{x}_1 = 0\}. \quad (68)$$

This set is the solution curve of (62) under the hypothesis that  $z_1$  remains constant. The other curve describes the set

$$\mathcal{S}_2(z_2) = \{(x_1, x_2) : \dot{x}_2 = 0\}. \quad (69)$$

This set is the solution curve of (63) under the hypothesis that  $z_2$  remains constant. The values of  $z_1$  and  $z_2$  can be held fixed because the trajectory is not near  $\mathcal{S}$  at the outset.

The set

$$\mathcal{S}(z_1, z_2) = \mathcal{S}_1(z_1) \cap \mathcal{S}_2(z_2) \quad (70)$$

describes the subset of  $\mathcal{S}$  that is reachable from  $\mathcal{F}$  given the initial values  $z_1$  and  $z_2$ . The set  $\mathcal{S}(z_1, z_2)$  consists of three points  $P_1$ ,  $P_2$ ,  $P_3$  in Fig. 13. These points are equilibrium points of  $(x_1, x_2)$  in the two-dimensional fast system  $\mathcal{F}$ . To determine how  $\mathcal{S}(z_1, z_2)$  is approached, we need to know the stability of these equilibrium points.

To analyse stability, note that set  $\mathcal{S}_1(z_1)$  is a set of points  $(x_1, x_2)$  which satisfy an equation of the form

$$x_1 = H(x_2, z_1). \quad (71)$$

Similarly, the set  $\mathcal{S}_2(z_2)$  satisfies an equation of the form

$$x_2 = H(x_1, z_2). \quad (72)$$

The same function  $H(x, z)$  appears in both equations due to the symmetry of (62) and (63).  $H(x, z)$  is single-valued if and only if

$$C_2 \leq 1 + C_1 + C_1/C_3. \quad (73)$$

The parameter values in Table 1 satisfy (73). If (73) is satisfied, then

$$\frac{\partial H}{\partial x} \leq 0. \quad (74)$$

An equilibrium point is stable if

$$\frac{\partial H}{\partial x}(x_1, z_2) \frac{\partial H}{\partial x}(x_2, z_1) < 1 \quad (75)$$

and is a saddle point if

$$\frac{\partial H}{\partial x}(x_1, z_2) \frac{\partial H}{\partial x}(x_2, z_1) > 1. \quad (76)$$

Using inequalities (75) and (76), we verify below that  $P_2$  is a saddle point, whereas  $P_1$  and  $P_3$  are stable

equilibrium points. Thus all trajectories that start off the one-dimensional stable manifold of  $P_2$  will be attracted to one of the stable equilibrium points  $P_1$  or  $P_3$ .

Equilibrium point  $P_1$  is stable because the graph of  $\mathcal{S}_2(z_2)$  is flat near  $P_1$ ; hence its slope  $\frac{\partial H}{\partial x}(x_1, z_2) = 0$  at  $P_1$ . Equilibrium point  $P_2$  is a saddle point because the graph of  $\mathcal{S}_2(z_2)$  has a slope  $\frac{\partial H}{\partial x}(x_1, z_2)$  with respect to  $x_1$ , whereas the graph of  $\mathcal{S}_1(z_1)$  has a slope

$$\frac{1}{\frac{\partial H}{\partial x}(x_2, z_1)} \quad (77)$$

when it is considered as a function of  $x_1$ . Figure 13 shows that

$$\frac{\partial H}{\partial x}(x_1, z_2) < \frac{1}{\frac{\partial H}{\partial x}(x_2, z_1)} \quad (78)$$

at  $P_2$ . Since both slopes in (78) are negative, (78) implies (76). The stability of  $P_3$  can be similarly determined.

Consider a trajectory that starts away from the set  $\{P_1, P_2, P_3\}$  and quickly jumps towards  $P_3$ . In the singular solution, the trajectory then lies in  $\mathcal{S}(z_1, z_2)$ . Once the trajectory is in  $\mathcal{S}(z_1, z_2)$ , the equations (66) and (67) governing the slow manifold  $\mathcal{S}$  take over and  $z_1$  and  $z_2$  slowly change. These changes cause the trajectory to move within  $\mathcal{S}$ . By Fig. 13,  $P_3$  lies at an  $(x_1, x_2)$  position where  $x_1$  is large and  $x_2$  is small. If  $z_1$  and  $z_2$  start at moderate values, then (66) causes a decrease in  $z_1$  while (67) causes an increase in  $z_2$ . These changes tend to cause an upward shift in the set  $\mathcal{S}_2(z_2)$  and a downward shift in the set  $\mathcal{S}_1(z_1)$ . As this shift in the sets takes place, the singular trajectory  $(x_1, x_2, z_1, z_2)$  continues to satisfy the constraint that  $(x_1, x_2) \in \mathcal{S}(z_1, z_2)$ .

The motion in  $\mathcal{S}$  can continue until the sets  $\mathcal{S}_1(z_1)$  and  $\mathcal{S}_2(z_2)$  become tangent (Fig. 14a) and then separate (Fig. 14b). When this occurs, the trajectory suddenly leaves  $\mathcal{S}$ . Its motion is then controlled by  $\mathcal{F}$ . By Fig. 14b, there is only one equilibrium point  $P$  in  $\mathcal{F}$  that can attract the trajectory at this time. By (75),  $P$  is a stable equilibrium point. A rapid jump of  $(x_1, x_2)$  to  $P$  thus occurs. Then the system is in  $\mathcal{S}$  again, but now  $x_1$  is small and  $x_2$  is large. Hence  $z_1$  tends to increase, thereby tending to drag  $\mathcal{S}_1(z_1)$  upward, and  $z_2$  tends to decrease, thereby tending to drag  $\mathcal{S}_2(z_2)$  downward until the trajectory is forced off  $\mathcal{S}$  onto  $\mathcal{F}$ , and the cycle repeats itself.

Two other outcomes are easily interpreted using this type of geometric description. It is possible for a

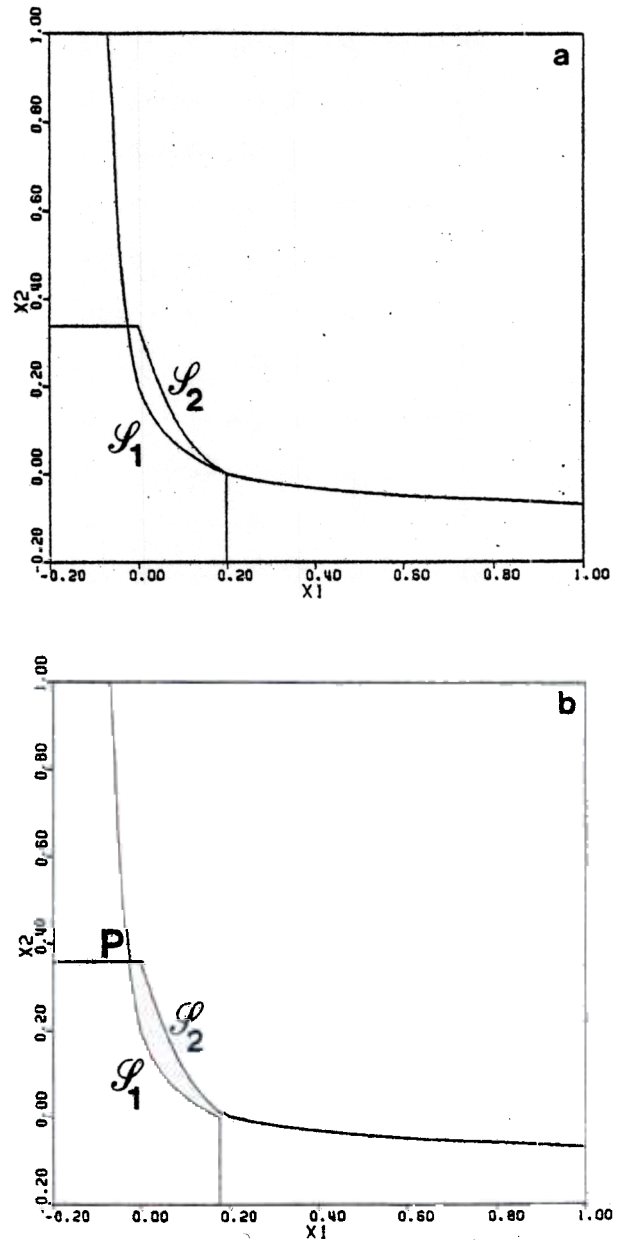


Fig. 14a and b. A jump off the slow manifold. In a,  $\mathcal{S}_1(0.3723)$  and  $\mathcal{S}_2(0.6074)$  are tangent. In b, slightly different  $z_1$  and  $z_2$  values cause the curves  $\mathcal{S}_1(z_1)$  and  $\mathcal{S}_2(z_2)$  to separate at their rightmost intersection, thereby forcing a jump within the fast manifold to  $P$ .  $\mathcal{S}_1(0.33)$  and  $\mathcal{S}_2(0.64)$  are graphed

motion in  $\mathcal{S}$  that starts at  $P_3$  to continue for all time. This will happen if  $\mathcal{S}_1(z_1)$  and  $\mathcal{S}_2(z_2)$  never become tangent, as in Fig. 14a. Then instead of jumping off  $\mathcal{S}$  into  $\mathcal{F}$ , the sets  $\mathcal{S}_1(z_1)$  and  $\mathcal{S}_2(z_2)$  can continue to shift slowly as the system approaches an off-diagonal limit.

By contrast, an intersection of  $\mathcal{S}_1(z_1)$  and  $\mathcal{S}_2(z_2)$  such as that depicted in Fig. 15 may also arise. Then  $\mathcal{S}(z_1, z_2)$  contains a single stable equilibrium point of  $\mathcal{F}$ . If this portrait persists, then an equilibrium point

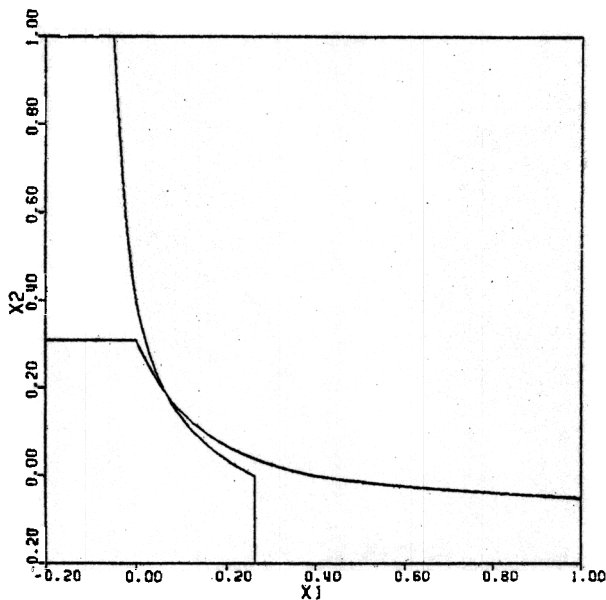


Fig. 15. A switch from  $\mathcal{F}$  to  $\mathcal{S}$  is followed by approach to a diagonal equilibrium point on  $\mathcal{S}$ . Parameters  $C_2$ ,  $C_3$ , and  $C_4$  are chosen as in Table 1. Parameter  $C_1 = 0.2$

on the diagonal is approached. Only a finite number of equilibrium points exist when the signal functions are threshold-linear.

The above geometrical description indicates the issues that need to be resolved to prove rigorous theorems about this system. For example, a complete understanding of how the sets  $\mathcal{S}_1(z_1)$  and  $\mathcal{S}_2(z_2)$  change as functions of  $z_1$  and  $z_2$ , given all possible choices of parameters, is needed. One also needs to know the location of the stable equilibrium points in  $\mathcal{S}(z_1, z_2)$  when  $\mathcal{S}_1(z_1)$  and  $\mathcal{S}_2(z_2)$  are tangent, and whether a jump in  $\mathcal{F}$  between a pair of these equilibrium points will cause  $z_1$  and  $z_2$  to increase or to decrease during the next motion within  $\mathcal{S}$ .

### 13 Concluding Remarks: Interdisciplinary Applications

This article analyzes the parametric structure of oscillations that can be generated by a gated pacemaker. Other articles in this series augment the gated pacemaker model with metabolic feedback and slow gain control processes that together help to explain difficult data such as split rhythms, several types of after-effects, Aschoff's rule and its exceptions, results of ablation studies and hormonal manipulations, and relationships between antidepressants and circadian rhythms (Carpenter and Grossberg, 1983a, b). The augmented circadian model is homologous to a model of the hypothalamic eating circuit (Grossberg, 1982a, 1983a). We believe that this homology illustrates how different hypothalamic circuits may be constructed from similar

mechanistic components (Olds, 1977). Thus the results herein about the circadian wake-sleep and activity-rest cycle may find application in studies of motivational rhythms (Rosenwasser et al., 1981). Gated dipole circuits have also been used to help analyse certain perceptual and cognitive phenomena (Grossberg, 1980, 1982b, 1983a, b). Although the rhythms that occur in these contexts are much faster than circadian rhythms, the same gated pacemaker circuit can be made to generate rhythms of essentially any period just by altering the dimensionless gain  $C_5$  of its transmitter gating process (Sect. 8). Thus the parametric studies reported herein may find their way into discussions of fast perceptual and cognitive rhythmic phenomena that seem to be unrelated to circadian rhythms, but on a mechanistic level may be properties of gated pacemaker circuitry.

### References

- Aschoff, J.: Influences of internal and external factors on the period measured in constant conditions. *Z. Tierpsychol.* **49**, 255-249 (1979)
- Carpenter, G.A.: A geometric approach to singular perturbation problems with applications to nerve impulse equations. *J. Diff. Eqs.* **23**, 335-367 (1977a)
- Carpenter, G.A.: Periodic solutions of nerve impulse equations. *J. Math. Anal. Appl.* **58**, 152-173 (1977b)
- Carpenter, G.A., Grossberg, S.: Adaptation and transmitter gating in vertebrate photoreceptors. *J. Theor. Neurobiol.* **1**, 1-42 (1981)
- Carpenter, G.A., Grossberg, S.: Dynamic models of neural systems: Propagated signals, photoreceptor transduction, and circadian rhythms. In: *Oscillations in mathematical biology*. Grissell, R., Hodgson, J.P.E., Yanowich, M. (eds.). Berlin, Heidelberg, New York: Springer 1983a
- Carpenter, G.A., Grossberg, S.: A neural theory of circadian rhythms: split rhythms, long-term after-effects, and Aschoff's rule (in preparation) (1983b)
- Daan, S., Pittendrigh, C.S.: A functional analysis of circadian pacemakers in nocturnal rodents. II. The variability of phase response curves. *J. Comp. Physiol.* **106**, 253-266 (1976)
- DeCoursey, P.J.: Phase control of activity in a rodent. *Cold Spring Harbor Symp. Quant. Biol.* **25**, 49-55 (1960)
- Earnest, D., Turek, F.W.: Splitting of the circadian rhythm of activity in hamsters: effects of exposure to constant darkness and subsequent re-exposure to constant light. *J. Comp. Physiol.* **145**, 405-411 (1982)
- Fitzhugh, R.: Impulses and physiological states in theoretical models of nerve membrane. *Biophys. J.* **1**, 445-466 (1961)
- Grossberg, S.: Some physiological and biochemical consequences of psychological postulates. *Proc. Natl. Acad. Sci.* **60**, 758-765 (1968)
- Grossberg, S.: Competition, decision, and consensus. *J. Math. Anal. Appl.* **66**, 470-493 (1978)
- Grossberg, S.: How does a brain build a cognitive code? *Psychol. Rev.* **87**, 1-51 (1980)
- Grossberg, S.: Psychophysiological substrates of schedule interactions and behavioral contrast. In: *Mathematical psychology and psychophysiology*. Grossberg, S. (ed.). Providence, R.I.: American Mathematical Society 1981

- Grossberg, S.: The processing of expected and unexpected events during conditioning and attention: a psychophysiological theory. *Psychol. Rev.* **89**, 529–572 (1982a)
- Grossberg, S.: Studies of mind and brain: Neural principles of learning, perception, development, cognition, and motor control. Boston: Reidel 1982b
- Grossberg, S.: Some psychophysiological and pharmacological correlates of a developmental, cognitive, and motivational theory. In: Brain and information: evoked potential correlates. Karrer, R., Cohen, J., Tueting, P. (eds.). New York: New York Academy of Sciences 1983a
- Grossberg, S.: The quantized geometry of visual space: the coherent computation of depth, form, and lightness. *Behav. Brain Sci.* (1983b) (in press)
- Gwinner, E.: Testosterone induces "splitting" of circadian locomotor activity rhythm in birds. *Science* **185**, 72–74 (1974)
- Hodgkin, A.L.: The conduction of the nervous impulse. Liverpool: Liverpool University 1964
- Hodgkin, A.L., Huxley, A.F.: A quantitative description of membrane current and its application to conduction and excitation in nerve. *J. Physiol.* **117**, 500–544 (1952)
- Hoffman, K.: Splitting of the circadian rhythm as a function of light intensity. In: Biochronometry. Menaker, M. (ed.). Washington, D.C.: National Academy of Sciences 1971, pp. 134–150
- Jouvet, M., Mouret, J., Chouvet, G., Siffre, M.: Toward a 48-h day: experimental bicircadian rhythm in man. In: Circadian oscillations and organization in nervous systems. Pittendrigh, C.S. (ed.). Cambridge, MA.: MIT Press 1974, pp. 491–497
- Kafka, M.S., Wirz-Justice, A., Naber, D., Marangos, P.J., O'Donohue, T.L., Wehr, T.A.: Effect of lithium on circadian neurotransmitter receptor rhythms. *Neuropsychobiol.* **8**, 41–50 (1982)
- Kafka, M.S., Wirz-Justice, A., Naber, D.: Circadian and seasonal rhythms in  $\alpha$ - and  $\beta$ -adrenergic receptors in the rat brain. *Brain Res.* **207**, 409–419 (1981)
- Kafka, M.S., Wirz-Justice, A., Naber, D., Wehr, T.A.: Circadian acetylcholine receptor rhythm in rat brain and its modification by imipramine. *Neuropharmacol.* **20**, 421–425 (1981)
- Katz, B.: Nerve, muscle, and synapse. New York: McGraw-Hill 1966
- Kawato, M., Suzuki, R.: Two coupled neural oscillators as a model of the circadian pacemaker. *J. Theor. Biol.* **86**, 547–575 (1980)
- Kramm, K.R.: Circadian activity in the antelope ground squirrel, *Ammospermophilus leucurus*. Ph. D. Thesis, University of California, Irvine 1971
- Kronauer, R.E., Czeisler, C.A., Pilato, S.F., Moore-Ede, M.C., Weitzman, E.D.: Mathematical model of the human circadian system with two interacting oscillators. *Am. J. Physiol.* **242**, R3–R17 (1982)
- Kuffler, S.W., Nicholls, J.G.: From neuron to brain. Sunderland, MA.: Sinauer 1976
- Moore, R.Y.: Retinohypothalamic projection in mammals: a comparative study. *Brain Res.* **49**, 403–409 (1973)
- Moore, R.Y.: Visual pathways and the central neural control of diurnal rhythms. In: Circadian oscillations and organization in nervous systems. Pittendrigh, C.S. (ed.). Cambridge, MA.: MIT Press 1974, pp. 537–542
- Moore-Ede, M.C., Sulzman, F.M., Fuller, C.A.: The clocks that time us. Cambridge, MA.: Harvard University Press 1982
- Naber, D., Wirz-Justice, A., Kafka, M.S.: Circadian rhythm in rat brain opiate receptor. *Neurosci. Lett.* **21**, 45–50 (1981)
- Nagumo, J., Arimoto, S., Yoshizawa, S.: An active pulse transmission line simulating nerve axon. *Proc. I.E.E.E.* **50**, 2061–2070 (1962)
- Olds, J.: Drives and reinforcements: behavioral studies of hypothalamic functions. New York: Raven Press 1977
- Pickard, G.E., Turek, F.W.: Splitting of the circadian rhythm of activity is abolished by unilateral lesions of the suprachiasmatic nuclei. *Science* **215**, 1119–1121 (1982)
- Pittendrigh, C.S.: Circadian rhythms and the circadian organization of living systems. *Cold Spring Harbor Symp. Quant. Biol.* **25**, 159–185 (1960)
- Pittendrigh, C.S.: Circadian oscillations in cells and the circadian organization of multicellular systems. In: Circadian oscillations and organization in nervous systems. Pittendrigh, C.S. (ed.). Cambridge, MA.: MIT Press 1964, pp. 437–458
- Plonsey, R.: Bioelectric phenomena. New York: McGraw-Hill 1969
- Pohl, H.: Characteristics and variability in entrainment of circadian rhythms in light in diurnal rodents. In: Vertebrate circadian systems. Aschoff, J., Daan, S., Groos, G.A. (eds.). Berlin, Heidelberg, New York: Springer 1982, pp. 339–346
- Rosenwasser, A.M., Boulos, Z., Terman, M.: Circadian organization of food intake and meal patterns in the rat. *Physiol. Behav.* **27**, 33–39 (1981)
- Sisk, C.L., Turek, F.W.: Role of the inter-connections of the suprachiasmatic nuclei in the hamster circadian system. *Soc. Neurosci. Abstr.* **8**, 35 (1982)
- Wehr, T.A., Wirz-Justice, A.: Circadian rhythm mechanisms in affective illness and antidepressant drug action. *Pharmacopsychiat.* **15**, 30–38 (1982)
- Wehr, T.A., Wirz-Justice, A., Goodwin, F.K., Duncan, W., Gillin, J.C.: Phase advance of the circadian sleep-wake cycle as an antidepressant. *Science* **206**, 710–713 (1979)
- Wever, R.A.: The circadian system of man: results of experiments under temporal isolation. Berlin, Heidelberg, New York: Springer 1979

Received: March 17, 1983

Dr. G. A. Carpenter  
Boston University  
Center for Adaptive Systems  
Mathematics Department  
264 Bay State Road  
Boston, MA 02215  
USA